iScience

CellPress
OPEN ACCESS

Article

Supramolecular DNA-based catalysis in organic solvents

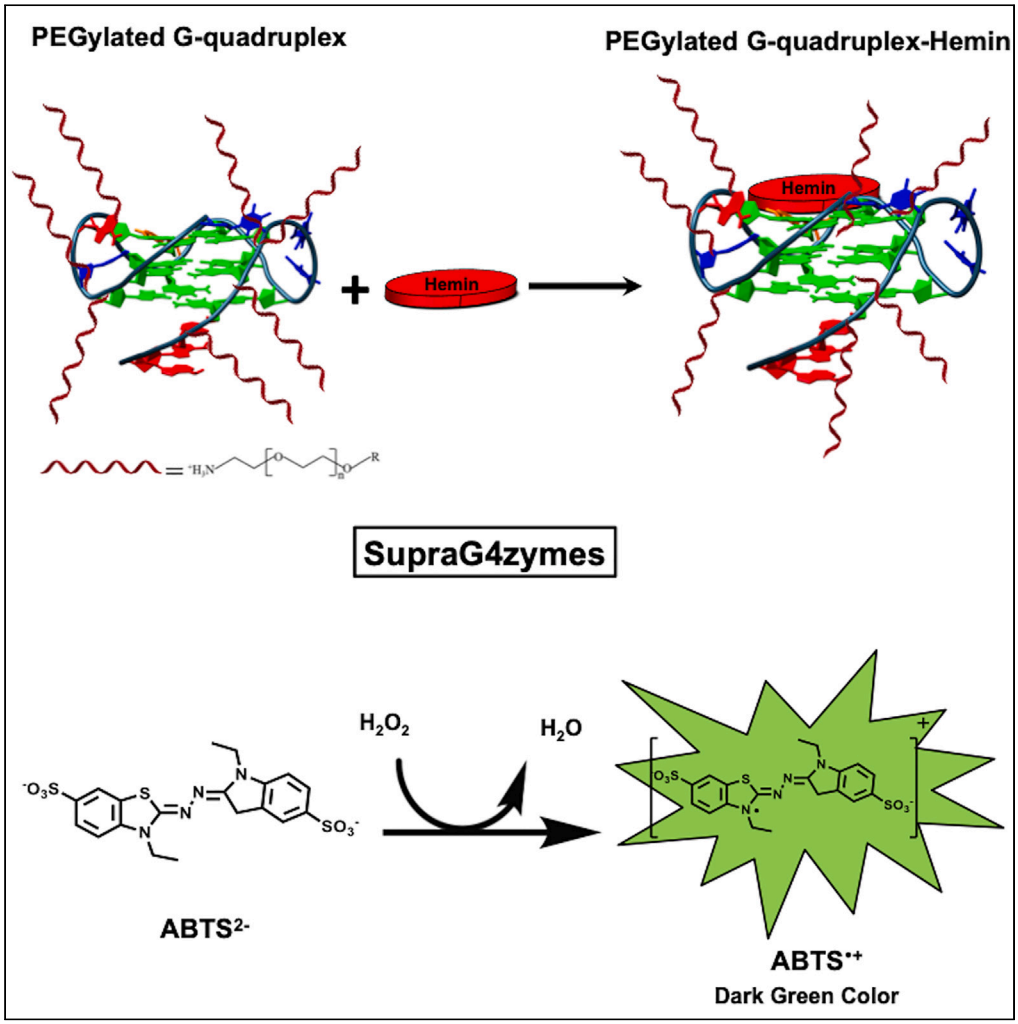

Gurudas Chakraborty, Konstantin Balinin, Rafael del Villar-Guerra, ..., Tanja Weil, Jonathan B. Chaires, Andreas Herrmann

herrmann@dwi.rwth-aachen.de

Highlights

High-density noncovalent PEGylation drives DNA solubility in polar organic solvents

G-rich DNA can form G-quadruplexes in a metal-free organic phase

Solvent-selective and structure-specific catalysis in organic solvents are demonstrated

Chakraborty et al., iScience 27, 109689
May 17, 2024
https://doi.org/10.1016/j.isci.2024.109689

iScience

CellPress
OPEN ACCESS

Article

Supramolecular DNA-based catalysis in organic solvents

Gurudas Chakraborty,[1,2] Konstantin Balinin,[1,2,3] Rafael del Villar-Guerra,[4] Meike Emondts,[2,5] Giuseppe Portale,[1] Mark Loznik,[1,2] Wiebe Jacob Niels Klement,[1] Lifei Zheng,[2] Tanja Weil,[3] Jonathan B. Chaires,[4] and Andreas Herrmann[1,2,5,6,*]

SUMMARY

The distinct folding accompanied by its polymorphic character renders DNA G-quadruplexes promising biomolecular building blocks to construct novel DNA-based and supramolecular assemblies. However, the highly polar nature of DNA limits the use of G-quadruplexes to water as a solvent. In addition, the archetypical G-quadruplex fold needs to be stabilized by metal-cations, which is usually a potassium ion. Here, we show that a noncovalent PEGylation process enabled by electrostatic interactions allows the first metal-free G-quadruplexes in organic solvents. Strikingly, incorporation of an iron-containing porphyrin renders the self-assembled metal-free G-quadruplex catalytically active in organic solvents. Hence, these "supraG4zymes" enable DNA-based catalysis in organic media. The results will allow the broad utilization of DNA G-quadruplexes in nonaqueous environments.

INTRODUCTION

The discovery of non-canonical secondary structures of DNA, in particular, G-quadruplexes (G4s) has significantly advanced the use of DNA from its conventional biological roles to remarkable applications in supramolecular chemistry and nanotechnology.[1] The unique potential of G-rich DNA strands to undergo self-assembly through Hoogsteen hydrogen bonding resulting in polymorphic tetrahelical structures[2–4] has led to their widespread implementation in the fabrication of several DNA-based systems including switches[5–7] and hydrogels.[8] Furthermore, the seminal discovery by Sen et al. unveiling the peroxidase-like activity of G-quadruplex-hemin complex (G4-h)[9] has immensely contributed toward various biosensing and bioanalytical applications.[10,11] This peroxidase-mimicking potential of G4-h has recently been employed for achieving localized polymerization of dopamine on the surface of DNA origami.[12]

All the above-mentioned contributions of G4s toward the advancement of DNA-centric technologies are limited to ion-rich aqueous media. The primary requirement for metal ions in solution stems from the polyanionic nature of the DNA backbone. The presence of nonspecifically bound monovalent or divalent metal-cations neutralizes the negative charges along the backbone of the polymer. This allows overcoming the repulsive Coulombic forces between the phosphates and enables folding into the native structure.[13,14] Moreover, metal ions stabilize the G4 structure by coordinating with the O6 atoms from G-tetrads (or G-quartets).[14–16] These quartets are elementary to the overall quadruplex topology. A computational study employing *ab initio* quantum chemical method reveals the positioning of a cation in the center provides an auxiliary stabilization to a G-tetrad.[17] All these facts categorically demonstrate the requirement of metal ions for the formation and stability of G4s.

The restriction in using G4s in organic solvents originates from the highly polar character of DNA molecules. Several methods are reported to solubilize DNA in organic media. The grafting of cationic lipophilic amphiphiles onto the phosphate anions of DNA[18] triggered the use of DNA in nonaqueous solvents. These organic soluble DNA-lipid complexes have been used to fabricate a variety of DNA-based materials including bulk films,[19–21] liquid crystals[22–24] and hydrogels.[25] The encapsulation of DNA with hydrophobic alkyl chains further allows DNA chemistry in organic media.[26,27] Apart from lipid-coated DNA, covalently conjugated DNA-polyethylene glycol (PEG) hybrid[28] and a simple DNA/PEG mixture[29] are soluble in selected organic solvents. Nanoparticles obtained from DNA and PEG-based synthetic cationic copolymers are also known to be soluble and stable in different organic solvents.[30] Furthermore, we have developed a ligand exchange process that facilitates electrostatic-decoration of DNA with the desired primary amine-functionalized surfactant resulting in a DNA complex soluble in organic media.[31] A method that relies on separating the oligonucleotide deprotection step from the cleavage process, contrary to the single-step cleavage/deprotection carried out soon after the solid-phase synthesis was recently reported for obtaining DNA in nonpolar organic media.[32]

[1]Zernike Institute for Advanced Materials, University of Groningen, Nijenborgh 4, Groningen 9747 AG, the Netherlands
[2]DWI-Leibniz Institute for Interactive Materials, Forckenbeckstraße 50, 52056 Aachen, Germany
[3]Max Planck Institute for Polymer Research, Ackermannweg 10, 55128 Mainz, Germany
[4]James Graham Brown Cancer Center, University of Louisville, 505 S. Hancock St., Louisville, KY 40202, USA
[5]Institute of Technical and Macromolecular Chemistry, RWTH Aachen University, Worringerweg 2, 52074 Aachen, Germany
[6]Lead contact
*Correspondence: herrmann@dwi.rwth-aachen.de
https://doi.org/10.1016/j.isci.2024.109689

Regardless of the availability of several approaches ensuring DNA solubility in the organic phase, limited research on the formation and activity of structured oligonucleotides (oligos) in organic solvents is known. Abe et al. have exemplarily demonstrated the use of covalently linked PEG-DNA conjugates for obtaining folded structures and catalytic activity of G-rich DNA dissolved in organic solvents.[28,33] Moreover, guanine nucleotides containing dodecyl groups result in a self-assembled tetramolecular hydrophobic G4 in chloroform.[34] The above investigations explicitly employ chemical methods for obtaining G4s in organic solvents. Such modification includes tedious synthesis and purification procedures. It necessitates an elaborate laboratory setup besides the substantial requirement for chemicals and solvents. Aside from using covalently conjugated hybrids of DNA, the cited literature has categorically emphasized on cation-induced structural changes in the obtained G4s.

To overcome the aforementioned synthetic challenges and broaden the applicability of DNA G4s in a variety of target environments, we for the very first time employ a noncovalent strategy for obtaining G4s in metal-free state and soluble in organic solvents. In this regard, the contribution from Wang et al. demonstrating the folding of hemin-terminated G-rich DNA in the aqueous medium into a catalytically active G4 topology, without the assistance of metal ions warrants mentioning.[35] However, the referred literature did not show any evidence that ensures a metal-free DNA backbone nor specifies the counterion that maintained the electrical neutrality of the employed sequence in the absence of metal ions. On the contrary, here the formation of G4s involves the folding of electrically neutral supramolecular architectures of G-rich DNA in polar protic organic media. The fabrication of such constructs relies on high-density grafting of positively charged PEG chains onto the negatively charged DNA backbone. This method renders metal-free DNA molecules and has earlier allowed obtaining thermally stable DNA duplexes in salt-free aqueous medium.[36] The present contribution unprecedentedly reports the fabrication of metal-free non-canonical DNA structures in organic solvents. To the best of our knowledge, obtaining DNA G4s in the absolute absence of metal ions either in organic or in aqueous media has never been demonstrated. Moreover, the resulting supramolecular G4 scaffolds together with hemin generate catalytically active species termed "supraG4zymes". The developed "supraG4zymes" empower DNA-mediated catalysis in organic solvents.

RESULTS

Synthesis and characterization of PEGylated DNA

PEG-encapsulated DNA (DNA-PEG) complexes were prepared according to the lately reported electrostatic PEGylation strategy.[36] The details concerning PEGylation and the sequences of the studied DNA oligos (ss22, CatG4, CatG4RR, PS2.M, and HT21) are mentioned in the STAR Methods section of the article. In brief, the formation of a DNA-PEG complex involves electrostatic complexation of the DNA with 4-(hexyloxy)anilinium (ANI) in the aqueous phase. This results in DNA precipitation. The obtained DNA-ANI complex was lyophilized followed by resuspension in methanol. Subsequently, an excess amount of amino-terminated methoxyPEG (mPEG-Amine) dissolved in methanol was added to the DNA-ANI solution. After ensuring the exchange of ANI molecules by cationic amino PEGs, the complex was washed to eliminate the untethered PEG and free ANI molecules. The final DNA-PEG complex was obtained after lyophilization. mPEG-Amine of 350 Da, 750 Da, and 2000 Da henceforth designated as PEG350, PEG750, and PEG2000, respectively, were used for obtaining various DNA-PEG constructs. All the complexes were characterized using proton nuclear magnetic resonance (^{1}H NMR) spectroscopy. Moreover, the grafting stoichiometry for each complex was determined following the previous literature.[36] For illustration, the ^{1}H NMR spectrum of pristine PEG350 (Figure S1) was compared to the spectrum of ss22-PEG350 complex (Figure S2). ss22-PEG350 displayed 63 protons corresponding to the terminal -CH_3 group of PEG350 but the same group in free PEG350 exhibited only 3 protons. The ratio of the number of protons associated with the specified -CH_3 group in the ss22-PEG350 complex to the ones in pristine PEG350 provides the density of grafting. The number of PEG chains tethered to the backbone of ss22, CatG4, CatG4RR, PS2.M, and HT21 were found to be 21, 20, 20, 17, and 20, respectively (Figures S2–S8). The obtained value for each complex corresponds to the net negative charge of the employed DNA. This ensures the encasing of the DNA with a PEG shell was achieved by the specific charge interaction between the DNA and PEG molecules (Figure 1A) as described in the referred article.[36]

Subsequently, the solubility of PEG-coated DNA (Figure 1B) in organic solvents was studied using the ss22-PEG350 complex. Organic solvents including methanol, ethanol, and dimethyl sulfoxide (DMSO) allowed obtaining 1.5 mM solutions of the PEGylated construct (Figure 1C). The comparison between the specified concentration and the previously reported solubility of covalent PEG-DNA hybrid[33] shows a 15 times increase in DNA solubility in organic media realized through electrostatic PEGylation. Further, the homogeneity in the acquired organic solutions was examined by recording the absorption spectra at various concentrations of ss22-PEG350. The peak at 260 nm characterizing the DNA absorbance was obtained for all the studied concentrations (1 μM–8 μM). The linear relationship between the absorbance at 260 nm and the corresponding concentration of ss22-PEG350 confirms the non-aggregated state of PEG-grafted DNA in organic solvents (Figure S9). Inductively coupled plasma optical emission spectrometry (ICP-OES) was used for the determination of metal ions in the PEGylated DNA solutions. The data concerning the concentrations of Na^+, K^+, and Mg^{2+} reveal the complete absence of metal-cations in the PEG-modified DNA (Table S1).

Metal-free formation of DNA G-quadruplexes in organic solvents

Following the characterization of the DNA-PEG complexes, PEGylated G-rich oligos dissolved in ultrapure water were subjected to annealing. The treated samples were further kept at 4°C for 2 h before lyophilization. The resulting materials were redissolved in the desired absolute organic solvents and allowed mixing for 1 h ensuring homogeneousness of the solutions. Further dilution of the DNA hybrids preceding their structural investigations was performed. The detailed procedure regarding the metal-free folding of PEG-decorated G-rich DNA strands is described in the STAR Methods.

The conformations of these folded species in the organic phase were mapped using circular dichroism (CD) spectroscopy. Oligos containing different base compositions and lengths, so-called CatG4, PS2.M, and HT21 were investigated. The rationale behind the selection was the

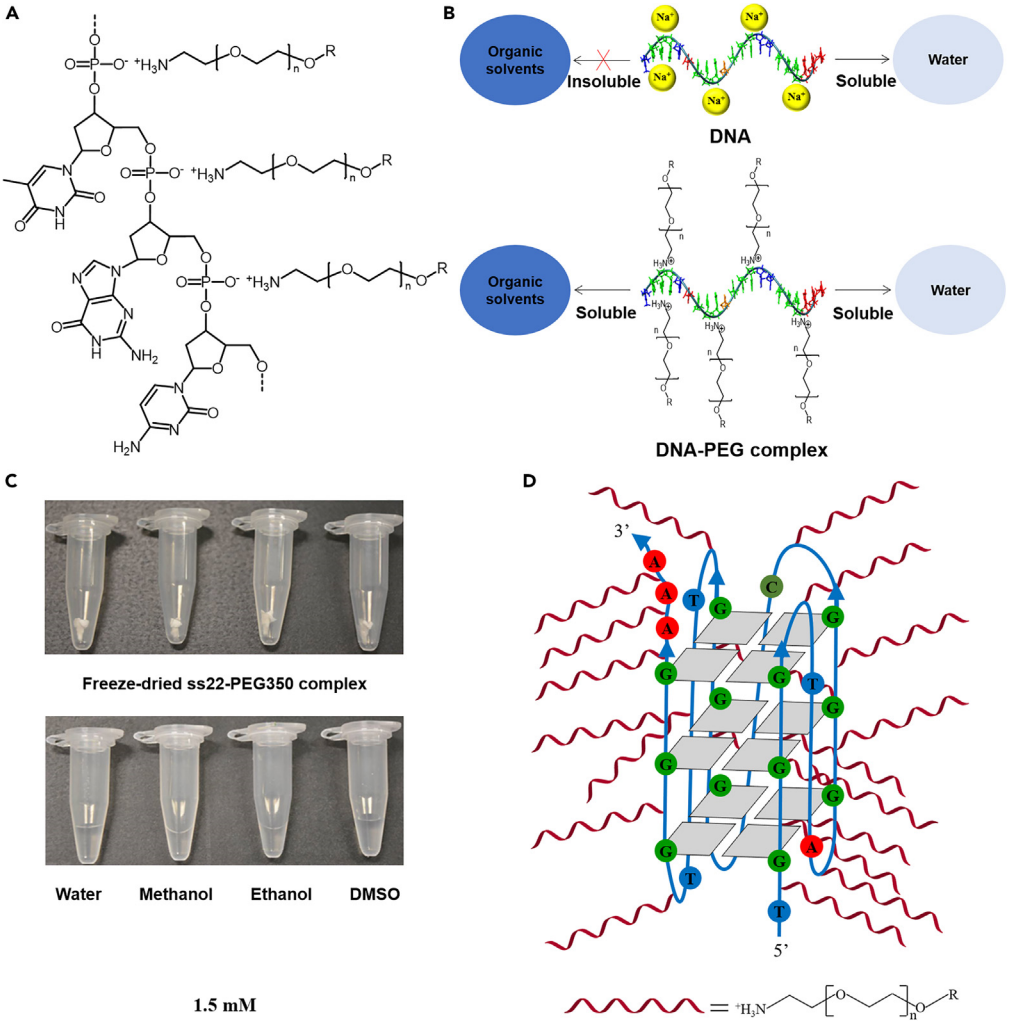

Figure 1. Schematic representation of PEG-modified DNA

(A) Molecular structure of a DNA-PEG complex showing specific charge interaction between the negatively charged phosphates of DNA and the cationic amino PEG chains.

(B) PEG-enveloped DNA is soluble in both organic solvents and water.

(C) 1.5 mM solutions of the ss22-PEG350 complex in various solvents.

(D) An illustration of an unimolecular G4 obtained by the folding of a PEG shelled G-rich DNA in metal-free organic medium.

inclusion of G-rich oligos that represent distinct folded topologies of DNA G4s. The mentioned strands result in intramolecular parallel, mixed type hybrid, and intramolecular antiparallel arrangements, respectively, in reported aqueous solutions.[37,38] The CD spectra of the afore-named oligos recorded under the previously defined conditions[37,38] henceforth served as the starting point for evaluating the conformational alterations occurring following PEGylation. Several factors including ionic strength of the solution, the dielectric constant of the solvent, choice of the metal ion, strand composition, and length contribute substantially toward the relative orientation of the participating strands.[39–41] Hence, these factors influence the final topology and different population of conformers present in solutions.[41]

CatG4 folded with K^+ exhibited a strong positive peak around 265 nm accompanied by a negative peak around 245 nm suggests the formation of a parallel conformation in the aqueous medium (Figure 2A).[37] In contradistinction, CatG4 grafted with PEG350 (CatG4-PEG350) dissolved in metal-free methanol displayed a positive band around 295 nm additionally to the two peaks stated above (Figure 2B). The obtained trait is indicative of an equilibrium between different G4 structures or the presence of a single mixed type hybrid quadruplex (Figure 3).[38,40] To ensure the spectrum of CatG4-PEG350 pertains to G-tract specific folding, CD of PEGylated strand containing randomly reorganized guanine bases designated as CatG4RR was recorded (Figure 2B). None of the spectral signatures featuring DNA G4s were observed.[37,38,40,42] This allows envisioning the folding of a PEG-tethered oligonucleotide containing tandem repeats of guanines in the typical quadruplex topology even in metal-cations deficit organic medium.

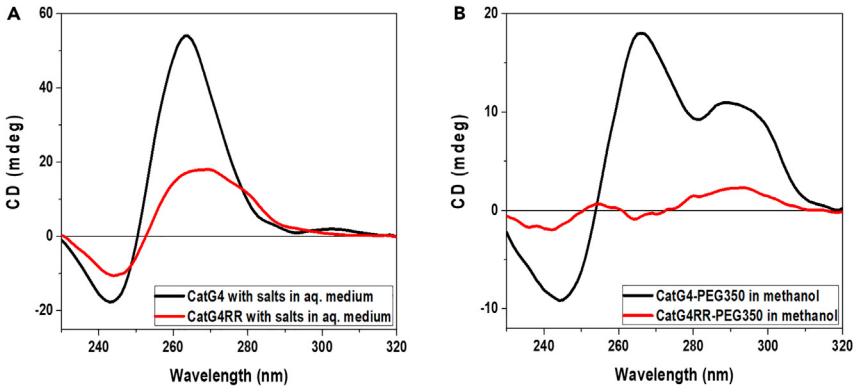

Figure 2. Mapping of pristine and PEG-grafted G-rich DNA using CD spectroscopy

(A) Spectra of 5 μM CatG4 (black) and CatG4RR (red), individually present in 10 mM Tris-HCl (pH 7.5), 1.6 mM KCl, and 0.8 mM $MgCl_2$.

(B) Spectra of 5 μM CatG4-PEG350 (black) and CatG4RR-PEG350 (red), separately dissolved in methanol.

The CD spectra of CatG4 encapsulated with PEG750 and PEG2000 labeled as CatG4-PEG750 and CatG4-PEG2000, respectively, in methanol further support the aforementioned observation (Figure S10). The non-aggregatable nature of PEG-grafted DNA following structuring in the organic phase was established by recording the CD spectra at various concentrations of CatG4-PEG350. An increase in the concentrations substantiated by the absorption spectra (Figure S11A) leads to a corresponding increase in the ellipticity (Figure S11B). A plot relating the circular dichroic properties, specifically at 265 nm with the employed concentrations of CatG4-PEG350 exhibits a linear correlation (Figure S11C). The homogeneity in the solutions is irrespective of the molecular weights of the mounted PEG chains (Figure S12).

Subsequently, the conformational properties of the above-specified hybrids were studied in ethanol (Figure S13). A substantial resemblance in the overall spectral pattern to the ones in methanol further corroborates the observed structural changes ensuing PEGylation, although their exact structures are yet to be determined. The folding of PEGylated G-rich DNA resulting in tetrahelical structure in organic solvents, specifically in the sheer absence of metal ions was further investigated using PS2.M and HT21. Similar to CatG4, the dominating parallel form of PS2.M in the buffer (Figure S14A) seems restructuring generating equilibrated conformers or topological concoction in its PEG tethered counterpart named PS2.M-PEG350 in methanol (Figure S14B) and ethanol (Figure S14C). Interestingly, the tertiary structure

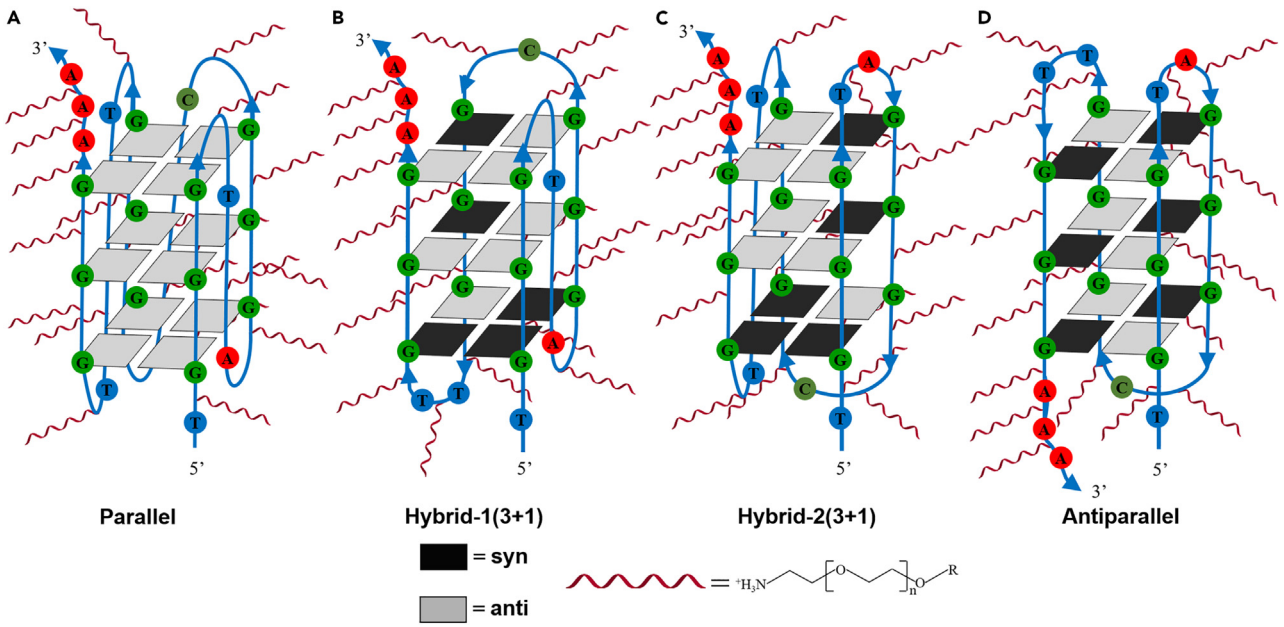

Figure 3. Illustration of various plausible quadruplex topologies of CatG4-PEG350 in the organic phase

(A) Parallel structure depicting the homostacks containing anti conformations of the guanines relative to the sugar in nucleotides.

(B and C) Two hybrid arrangements involving syn and anti-guanines.

(D) Antiparallel conformer displaying heterostacking of alternating syn/anti guanine bases.

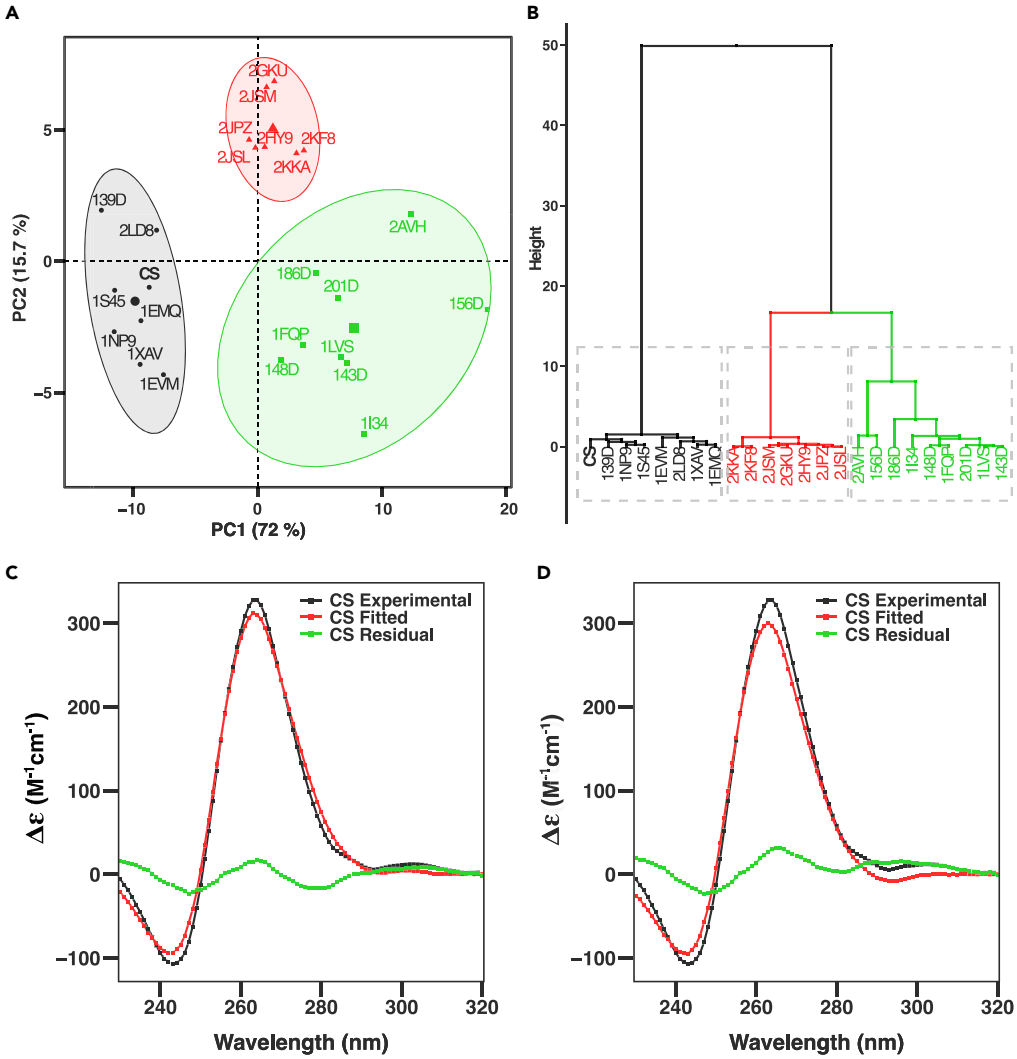

Figure 4. Quantitative analysis of 5 μM CatG4 present in 10 mM Tris-HCl (pH 7.5), 1.6 mM KCl, and 0.8 mM $MgCl_2$ (CS) CD spectrum

(A) Unbiased sorting of CS during PCA based upon the overall shape of its spectrum is represented as a score plot.

(B) HCA dendrogram demonstrating the clustering of CS to the well-known parallel G4 structures.

Black, green, and red shaded ellipses in the score plot (A) and clusters in the dendrogram (B) represent parallel, antiparallel, and "hybrid" or 3 + 1 topologies, respectively.

(C) Assessment of the secondary structural elements that include *anti-anti, syn-anti, anti-syn* dinucleotide steps, lateral and diagonal loops along with other residual structures.

(D) Estimation of the parallel, hybrid, and antiparallel tertiary conformations.

of HT21 in aqueous solution was largely retained in organic media. A strong positive peak around 295 nm typifying the antiparallel arrangement[43] was noted in all the cases, though their shape varied moderately between 240 and 280 nm (Figure S15).

Quantification of the circular dichroism spectra

The conformational changes following PEGylation have stimulated quantifying the experimental CD spectra for obtaining the secondary structure as well as topological information. The spectra of the samples containing triplet repeats of guanines (Table S2) were analyzed. The evaluation employs a recently developed analytical method.[44] The acquired spectra were subjected to principal component analysis (PCA) and hierarchical cluster analysis (HCA) using a curated CD spectra library of widely known G4 structures. An unbiased sorting during PCA basing upon the overall shape of the obtained CD spectra was performed. The conformational group allocation was done by comparing the test spectra with the reference spectra clusters (Figure S16).

The PCA (Figure 4A) and cluster analysis (Figure 4B) show that the CD spectrum of CatG4 obtained in the salt-rich aqueous medium (CS) is grouped to the well-known parallel G4 structures (black). This analysis suggests the complete parallel orientation of the

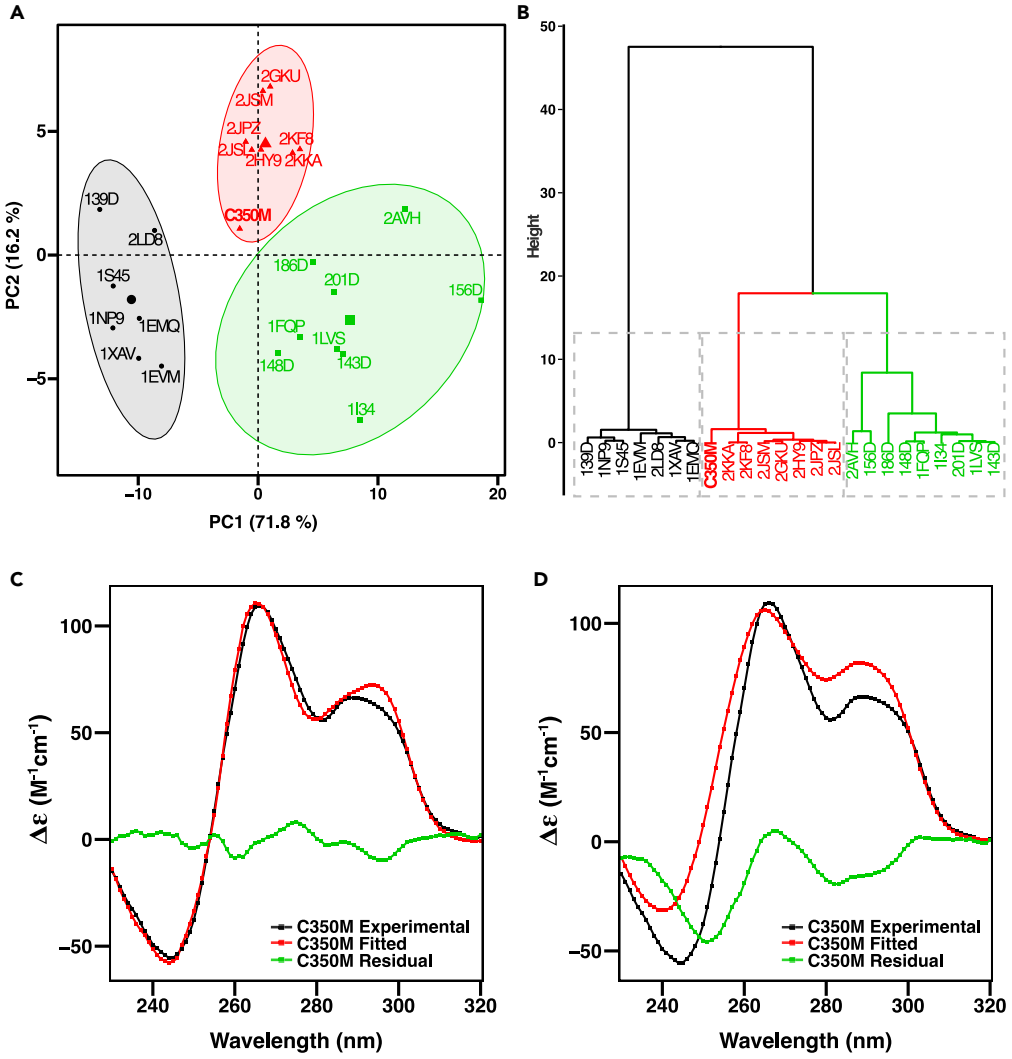

Figure 5. Quantitative evaluation of 5 μM CatG4-PEG350 dissolved in methanol (C350M) CD spectrum

(A) PCA score plot representing the unbiased sorting of C350M based upon the acquired shape of its spectrum.

(B) Dendrogram obtained by hierarchical clustering shows the presence of C350M at the edge of the widely known hybrid G4 structure group.

Parallel, antiparallel, and "hybrid" or 3 + 1 topologies in the score plot (A) and dendrogram (B) are shown in black, green, and red, respectively.

(C) Estimation of the fractions of the secondary structure contents such as *anti-anti*, *syn-anti*, *anti-syn* dinucleotide steps, lateral and diagonal loops as well as other residual structures.

(D) Determination of the tertiary components that include parallel, hybrid, and antiparallel topologies.

CatG4 strands under the studied condition. However, the spectrum of CatG4-PEG350 in methanol (C350M) is located close to the center of the PCA plot (Figure 5A) and at the edge of the hybrid G4 structure group (red) in the cluster analysis (Figure 5B). The localization of C350M close to the origin of coordinates in the PCA plot suggests the existence of at least a mixture of three components in methanol. Approximate assessments of the fractions including *anti-anti*, *syn-anti*, *anti-syn* dinucleotide steps, lateral and diagonal loops along with other residual structures were done (Table S3). The percentage of contributions from parallel, hybrid, and antiparallel conformers were further determined (Table S4). These secondary and tertiary structural elements were estimated using a reported set of basis spectra for fitting the measured CD spectra. The fitting providing secondary parameters of CS (Figure 4C) and C350M (Figure 5C), as well as tertiary information concerning CS (Figure 4D) and C350M (Figure 5D), was executed. On the basis of PCA, cluster analysis, and fitting performed (Figures S17–S27), each examined sample was assigned with the most relevant quadruplex structure from the library used (Table S5).

Notably, a linear increase of the parallel conformers with increasing molecular weights of the grafted PEG chains was observed for PEGylated CatG4 in both methanol and ethanol (Table S4). Furthermore, a comparison involving CatG4 complexed with PEG of particular

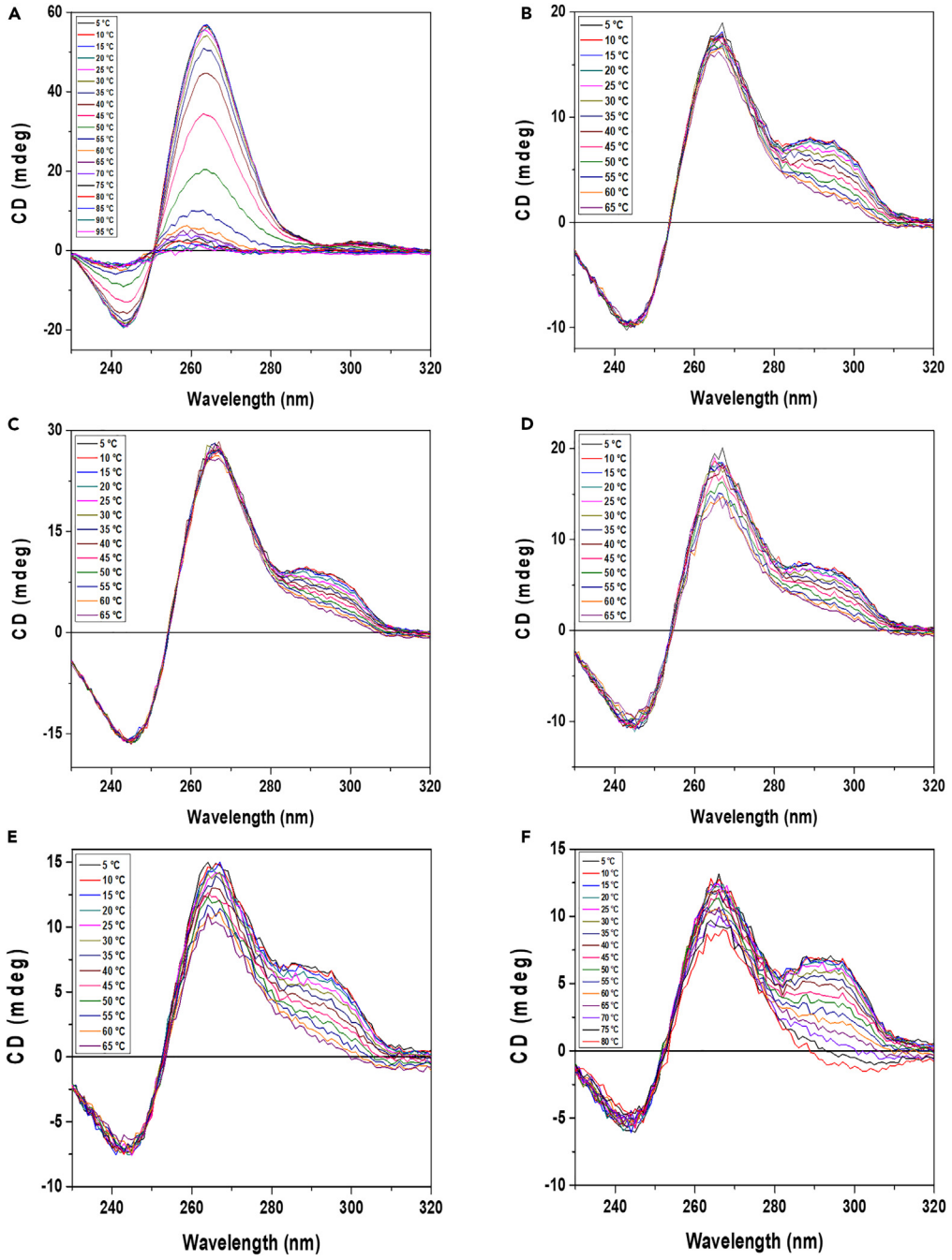

Figure 6. CD melting experiments of non-PEGylated and PEGylated G-rich DNA structures

(A) 5 μM CatG4 present in 10 mM Tris-HCl (pH 7.5), 1.6 mM KCl, and 0.8 mM $MgCl_2$.

(B) 5 μM CatG4-PEG350 in methanol.

(C) 5 μM CatG4-PEG750 in methanol.

(D) 5 μM CatG4-PEG2000 in methanol.

(E) 5 μM PS2.M-PEG350 in methanol.

(F) 5 μM PS2.M-PEG350 in ethanol.

molecular weight in methanol and ethanol shows a higher percentage of discrete parallel/antiparallel conformers in ethanol. The hybrid structure seems to be dominant in methanol. Further studies on the effects of PEG molecular weights and solvents governing the folding of the PEGylated DNA strands in metal-free organic media are beyond the scope of the present research and will be dealt with separately.

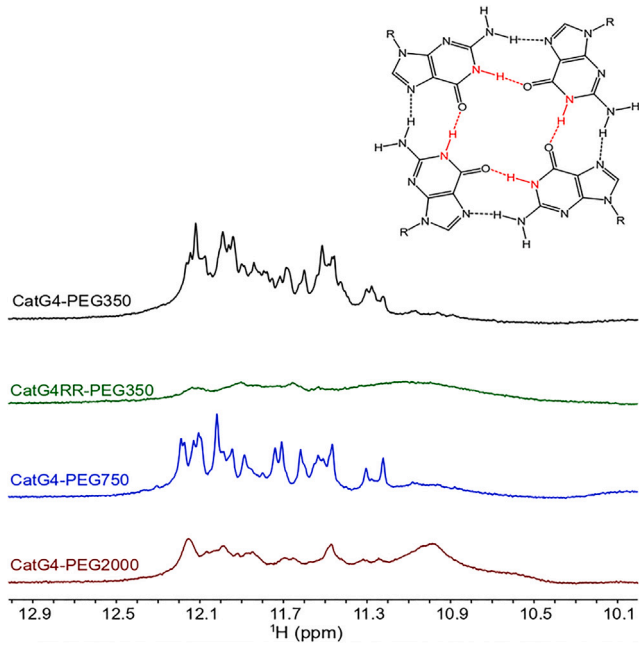

Figure 7. 1D ^{1}H NMR-based investigation of the imino region of the PEGylated G-rich DNA in methanol-d_3 (CD_3OH, 600 MHz)

Comparison between CatG4-PEG350 (black), CatG4RR-PEG350 (green), CatG4-PEG750 (blue), and CatG4-PEG2000 (dark red) imino protons (shown in red in the inserted chemical structure of a G-quartet) spectra.

Temperature-induced changes in the PEGylated structures

The alterations in the circular dichroic properties reflecting the structural transitions occurring due to the application of heat[42] to the samples having periodic repeats of guanines were monitored. A gradual reduction in the ellipticity at 265 nm with increasing temperature was observed for CatG4 with salts in the aqueous medium (Figure 6A) whereas CatG4-PEG350 in methanol showed no decrease at the indicated wavelength (Figure 6B). However, a decrease in the ellipticity at 295 nm was noticed. This could be due to the selective destabilization of the antiparallel conformations from the topological blend in the organic phase. The effect of the molecular weight of the polymer shell on the thermal stability of the PEG-coated structures was then investigated in methanol. CatG4-PEG750 (Figure 6C) behaved similarly to CatG4-PEG350 but CatG4-PEG2000 exhibited reduced ellipticities at 265 nm besides 295 nm (Figure 6D). Such a decrease in ellipticities indicates lesser stability conferred to the resulting quadruplex molecules by the longer PEG chains. Interestingly, none of the PEGylated structures experienced complete unfolding as witnessed for the non-PEGylated CatG4.

These findings were verified further by performing the melting experiments in ethanol (Figure S28). A considerable similarity in the acquired profiles of the tested hybrids to the corresponding ones in methanol was found. The mentioned observations explicitly establish the folded shape with enhanced stability of the designed supramolecular DNA G4s. The difference in the monitored temperature ranges for the aqueous and organic systems is due to the different boiling points of the employed solvents.[45] The importance of the length and nucleotide composition on the stability of PEGylated G4s was realized by comparing the unfolding of PS2.M-PEG350 with CatG4-PEG350. Although notable differences characterizing the structural changes appeared, the completely unfolded structure of PEG-chained PS2.M remained yet unobserved (Figures 6E and 6F).

Imino proton NMR spectra of the G-quadruplexes in the organic phase

Furthermore, the Hoogsteen base-pairing involved in the metal-free fabrication of the PEGylated DNA G4s in organic solvents was established recording the characteristic imino peaks employing ^{1}H NMR spectroscopy. The imino protons associated with guanines in G-quartet formation result in sharp and well-resolved idiosyncratic chemical shifts at around 10.5 to 12.0 ppm.[46] This region is separated from the imino chemical shifts of single-stranded oligos, double-helical, or other secondary structures of DNA.[47]

Strong proton signals in the aforementioned region appeared for CatG4-PEG350 whereas CatG4RR-PEG350 displayed no such chemical shift of the imino protons (Figure 7). This is a strong indicator for the specific folding of the PEG-bound G-rich DNA supramolecules. Subsequently, the influence of the PEG casing on the imino protons was monitored using various PEGylated complexes of CatG4. CatG4-PEG750 showed peaks resembling CatG4-PEG350 but the signals for CatG4-PEG2000 were comparatively blunt and less resolved (Figure 7). This could potentially be attributed to the shielding imposed by the longer PEG chains. The lengths of the PEG grafts seem to affect the splitting pattern of the imino peaks as well. Further validation regarding the involvement of Hoogsteen hydrogen bonds in the construction of DNA G4s in organic media was done by recording the imino proton spectra of PS2.M-PEG350 and HT21-PEG350 (Figure S29). The difference in the nature of imino peaks

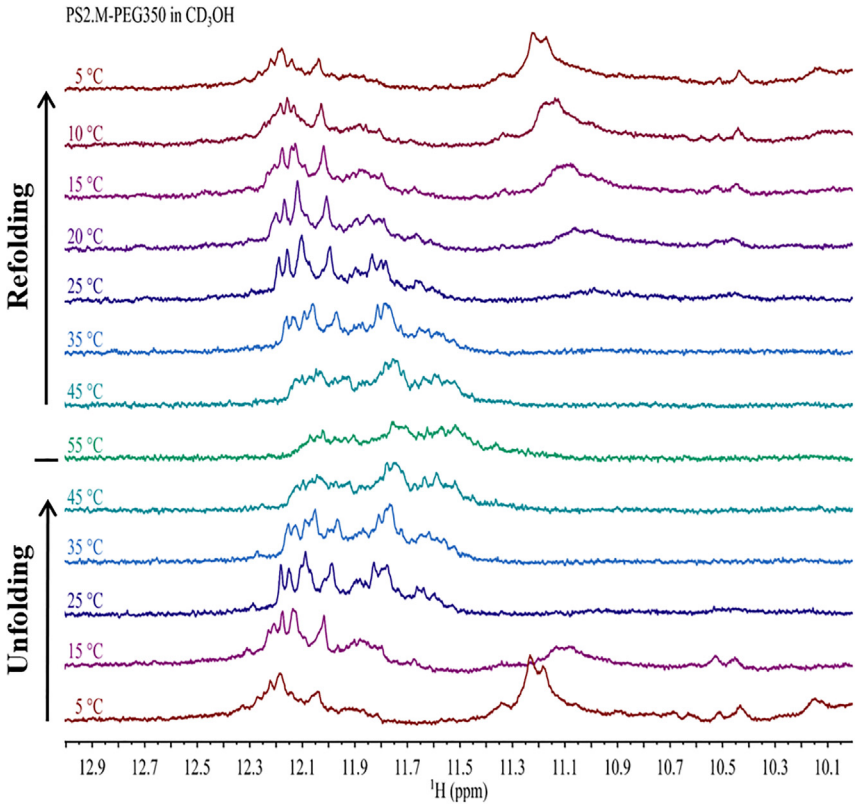

Figure 8. 1D ^{1}H NMR-based analysis of the thermal robustness of the PEGylated DNA G4 in methanol-d_3 (CD_3OH, 600 MHz)

Temperature-induced unfolding (bottom 5°C–55°C) and refolding (55°C to top 5°C) reflected by monitoring the changes in the imino region of PS2.M-PEG350.

of CatG4-PEG350, PS2.M-PEG350, and HT21-PEG350 unveils the effect of the primary nucleotide sequence on the obtained quadruplex structures[48] (Figure S30). In addition, the thermal robustness of the PEGylated G4s in the organic phase was demonstrated by monitoring temperature-dependent changes in the imino region of PS2.M-PEG350 (Figure 8). An apparent fall in the signal intensity at elevated temperatures and their reappearance by lowering the temperature demonstrates the unfolding and refolding of the designed structure, respectively. The complete loss of the imino proton signal remained undetected corroborating the inference of the CD melting experiments.

Solution small-angle X-ray scattering profiles of electrostatically PEGylated G-quadruplexes

Following the above spectroscopic characterizations, small-angle X-ray scattering (SAXS) was employed for investigating further the folded structures in organic solvents. SAXS is an established tool for studying the size and shape of biological macromolecules in solution.[49] Initially, the scattering profile of pristine CatG4 annealed in salt-rich aqueous medium was recorded for obtaining the structural characteristics associated with DNA G4s (Figure 9A). The plateau in the low-q region followed by downwards concave feature observed in the log(I(q)) vs. log(q) plot suggests the presence of compact, folded globular particles.[50,51] The radius of gyration (R_g) of CatG4 was then determined using Guinier analysis[50] (Figure S31A). The obtained value of 1.4 nm was further verified by direct intensity fitting[52] (Figure S31B) and by the computation of the so-called pair distance distribution function, $P(r)$[53] (Figure S31C). Additionally, the $P(r)$ allowed the estimation of the maximum dimension (D_{max}) of CatG4 that was found to be 4.5 nm. The symmetric bell-shaped trend of the $P(r)$ confirms the globular compact shape adopted by the CatG4 biomacromolecule.[49] The close-packed structure of CatG4 was also confirmed by the Kratky analysis of the acquired scattering data (Figure 9B). The pronounced single peak in $I(q)*q^2$ vs. q plot is an explicit indicator of compact scattering objects,[50,54] consistent with CatG4 adopting a folded topology.

Subsequently, the SAXS profiles of PEGylated CatG4 in organic solvents were recorded. CatG4-PEG350 generated an arc-shaped profile translating into a broad peak in the region lying between $0.5\ nm^{-1} \leq q \leq 2.0\ nm^{-1}$ in methanol (Figure 9C) as well ethanol (Figure S32A), similar to the scattering pattern of the quadruplex formed by unmodified CatG4 in the aqueous milieu. Moreover, an overall resemblance of the Kratky plots in methanol (Figure 9D) and ethanol (Figure S32B) regarding the appearance of a broad peak, as observed for the CatG4 substantiates the folded structure of CatG4-PEG350. The R_g of 1.3 nm calculated from the intensity fitting of the CatG4-PEG350 scattering data (Figure S33) agrees closely to the CatG4 R_g and thereby serves as auxiliary evidence for the metal-free structuring of electrostatically PEGylated oligos in the organic phase.

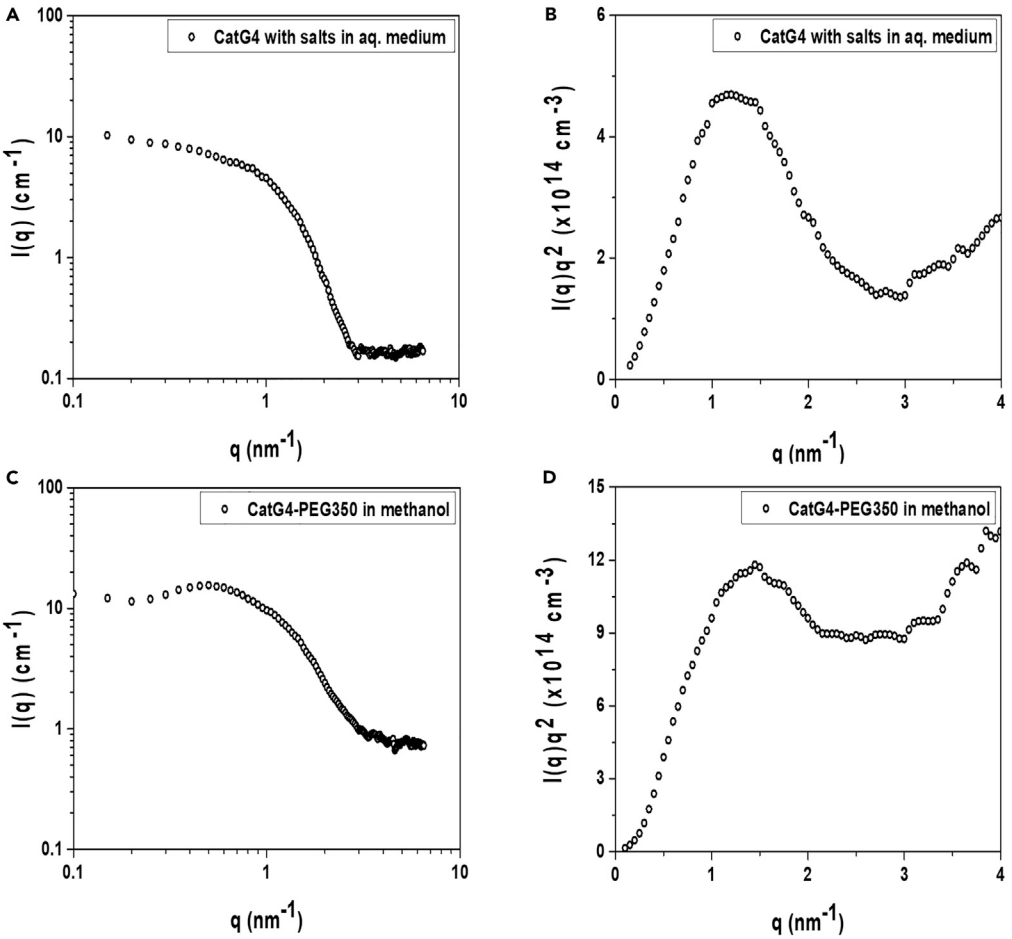

Figure 9. SAXS-based structural investigations of non-PEGylated and PEGylated CatG4

(A) Scattering profile of 0.4 mM CatG4 present in 50 mM Tris-HCl (pH 7.5), 100 mM KCl, and 5 mM $MgCl_2$.

(B) Kratky plot of CatG4.

(C) Scattering pattern of 0.4 mM CatG4-PEG350 dissolved in methanol.

(D) Kratky plot of CatG4-PEG350.

Importance of organic solvents for the formation of a PEGylated DNA G-quadruplex

The significance of organic medium for the metal-free folding of a PEG-shelled G-rich DNA into a G4 structure was subsequently examined. The investigation includes the comparison of the CatG4-PEG350 spectroscopic data obtained in methanol to that in ultrapure water. CatG4-PEG350 dissolved in ultrapure water was annealed and kept at 4°C for 2 h. The sample was then diluted and its structural characterization was performed. A considerable decrease in the signal intensity along with the hypsochromic shift in the CD spectrum of CatG4-PEG350 recorded in ultrapure water in comparison to the spectrum in methanol was observed (Figure S34A). Moreover, no spectral features typical to DNA G4s[37,38,40,42] were obtained for the sample in ultrapure water. These observations suggest the absence of the G4 structure in ultrapure water. This was further verified by ^{1}H NMR spectroscopy. No characteristic peaks of DNA G4s[46] were detected in the imino proton spectrum acquired in H_2O/D_2O mixture (Figure S34B). The appearance of a "hump" around 10.9 ppm further indicates the sequence is mostly unfolded in the employed aqueous milieu.[55] Such medium selective structure formation demonstrates the important role of solvent dielectric constant for the folding of a PEGylated G-rich DNA in the absence of metal ions. Further research on solvent-induced structuring of DNA-based supramolecules is beyond the scope of the present study and will be discussed in a separate article.

DNA-based catalysis in the organic phase

The fact, that iron-containing porphyrins bind to DNA G4s in aqueous solution and are catalytically active in regard to oxidation reactions with peroxidase-like activity is well-documented.[9,38] The addition of 20–30% v/v of a protic solvent such as methanol or formamide to aqueous solutions is further known to enhance the aforementioned oxidative property of hemin-bound DNA G4s.[56] Moreover, engineered biomolecular catalysts have long served in developing reactions and processes with environmental stewardship.[57] These accomplishments inspired us

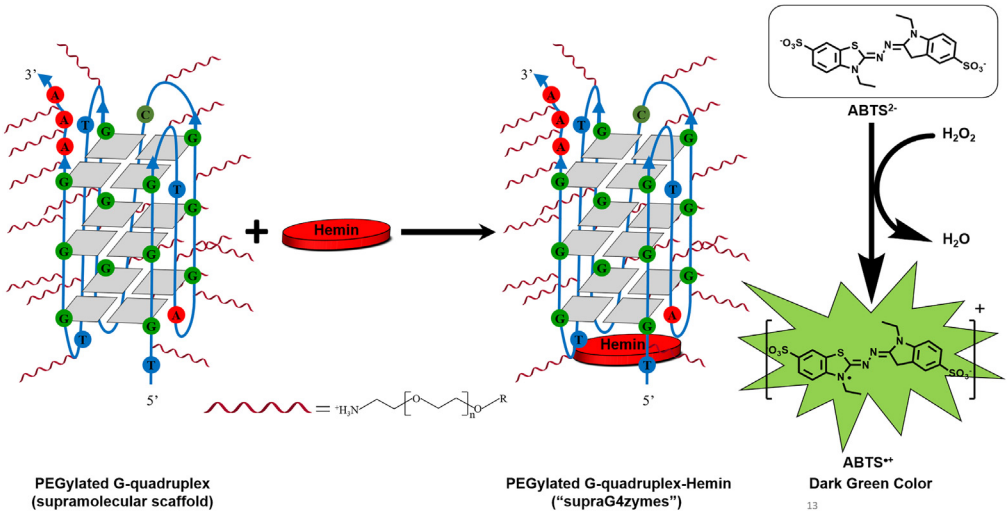

Figure 10. Schematic representation of supramolecular DNA-based catalysis in organic solvents

Oxidation of ABTS by H_2O_2 in the presence of a PEGylated G-quadruplex-hemin complex.

to investigate the catalytic functionality of hemin-containing, noncovalently PEGylated, G-rich suprabiomolecular scaffolds in polar protic organic solvents. The activity was monitored using a chromogenic substrate, 2,2′-azino-bis(3-ethylbenzothiazoline-6-sulphonic acid) (ABTS) (Figure 10). In the presence of a G4-hemin complex and hydrogen peroxide (H_2O_2), ABTS can be oxidized into $ABTS^{\cdot+}$ that exhibits a dark green color and hence enables colorimetric monitoring of the reaction kinetics.[58,59]

Employing CatG4-PEG350 under these conditions revealed a characteristic peak at 414 nm in the absorbance spectra demonstrating $ABTS^{\cdot+}$ formation[37] in methanol (Figure 11A) and ethanol (Figure S35A). Subsequently, time-dependent absorbance changes at 414 nm were recorded. The kinetic measurements were performed immediately after the addition of H_2O_2 in methanol (Figure 11B) and ethanol (Figure S35B). These assays unveil the peroxidase-like activity of the CatG4-PEG350 in organic solvents. We termed these catalytically active self-assembled supramolecular DNA G4s "supraG4zymes". The activity in ethanol was found to be lower than that in methanol (Figure S36). Although the elucidation of the exact underlying reason needs further research, this solvent-selective catalytic behavior could primarily be attributed to the difference in the radical generation ability and their stability in the employed alcohols.[60,61] CatG4 and CatG4RR-PEG350, serving as negative controls, showed no catalytic activity similar to the system without CatG4-PEG350 in methanol. This was due to the limited solubility of the unmodified DNA in the absolute organic phase and absence of a G4 structure (vide supra), respectively.

Intramolecular parallel G4 structures possess higher peroxidase activity than coexisting or mixed-type hybrids whereas the intramolecular antiparallel structure exhibits weak activity in aqueous medium.[38] Such structure specificity in the activity of the "supraG4zymes" was demonstrated by comparing the oxidation profiles of the coexisting or mixed-type hybrid CatG4-PEG350 and the dominantly antiparallel HT21-PEG350 in methanol. CatG4-PEG350 showed substantially higher activity than HT21-PEG350 in both spectra (Figure 11C) and time-course measurements (Figure 11D). Higher activity was also observed for CatG4 in comparison to HT21 in the aqueous medium (Figure S37). But establishing a direct comparison of the activity in aqueous and organic media should be abstained owing to the aforementioned underlying differences in the structural aspect of the DNA component of the employed biocatalysts. Subsequently, the influence of the molecular weight of the PEG shell on the catalytic performance of the PEGylated structures was examined. CatG4-PEG750 displayed higher activity than CatG4-PEG350 in methanol (Figure S38). This increase could potentially be ascribed to the increased percentage of parallel conformation with an increase in the molecular weight of the grafted PEG chains, as observed from the tertiary structure analysis (Table S4) described above. A further increase in the molecular weight of the PEG chains to 2000 Da does not increase the peroxidase activity despite an increase in the percentage of parallel conformation among the mixture of topologies. The activity of CatG4-PEG2000 was found to be slightly lower than that of CatG4-PEG750 but is noticeably higher than CatG4-PEG350 in methanol (Figure S39). This might be due to the steric hindrance imposed by the longer PEG chains encapsulating the DNA that limits the accessibility of the substrate molecules. The kinetics involved in "supraG4zymes"-catalyzed reaction in a polar protic organic phase were quantitatively realized by obtaining the maximum rate (V_{max}) and the Michaelis constant (K_m) values of CatG4-PEG350-hemin complex-catalyzed ABTS oxidation in methanol using the classical *Michaelis-Menten* equation (Equation 1).[38,62] The kinetic parameters, V_{max} and K_m, were determined to be 24.36 $\pm$ 1.57 nMs^{-1} and 0.370 $\pm$ 0.087 mM, respectively (Figure S40). The dependence of the initial rate (V_0) of the aforesaid reaction on the substrate concentration is shown in Table S6.

Furthermore, the effect of the G-rich scaffold on the oxidation of the substrate was investigated. The "supraG4zymes" obtained by an increase of CatG4-PEG350 at a fixed hemin concentration attaining 1:1, 5:1, 10:1, and 20:1 scaffold to the cofactor ratio were allowed to oxidize 1 mM ABTS in methanol. A consistent increase in the $ABTS^{\cdot+}$ formation was favored by the increased CatG4-PEG350 concentration, as

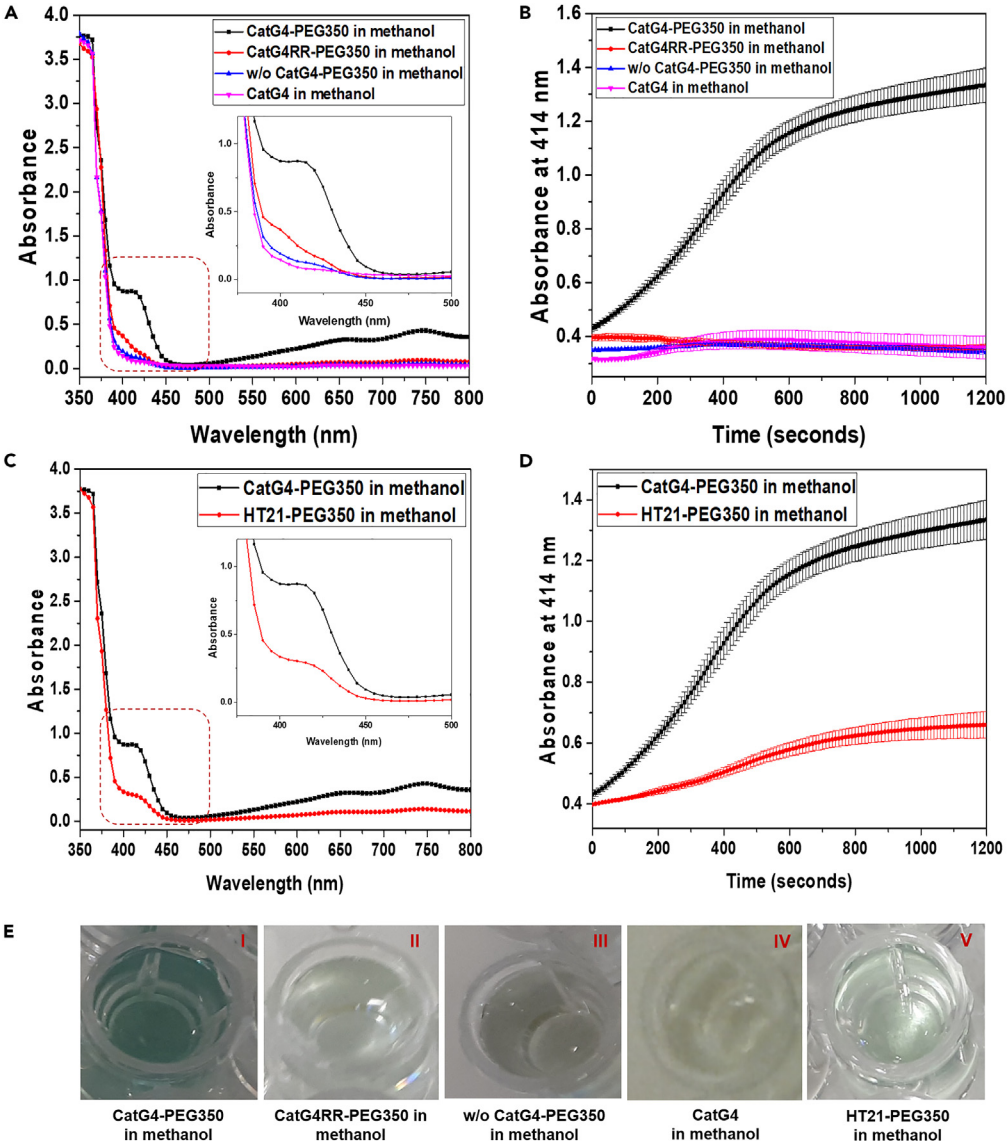

Figure 11. Catalytic activity of electrostatically engineered and unmodified DNA G-quadruplexes in methanol

(A) Absorbance spectra demonstrating $ABTS^{\cdot+}$ formation in the presence of CatG4-PEG350.

(B) Time-dependent absorbance changes at 414 nm confirming the peroxidase-like activity of the CatG4-PEG350.

(C) Absorbance spectra showing a higher activity of the coexisting or mixed-type hybrid CatG4-PEG350 in comparison to the dominantly antiparallel HT21-PEG350.

(D) Time-course measurements validating structure-specific activity of the "supraG4zymes".

(E) Photographs reflecting on the status of ABTS oxidation in different reaction mixtures.

reflected by the absorbance-based assays (Figure S41). This could be due to the generation of more active catalytic species by maximizing the use of the unbound hemin molecules upon the availability of more DNA at higher ratios. The restrictions on the effective interaction of the cofactor with the supramolecular scaffold seem to have been levied by the PEG grafts. To establish the generality of peroxidase-like activity of "supraG4zymes" in regard to oxidation reactions, the oxidation of 10-acetyl-3,7-dihydroxyphenoxazine (Amplex Red), catalyzed by CatG4-PEG350-hemin complex was executed in methanol (Figure S42). All the aforesaid findings unequivocally establish supramolecular DNA-mediated catalysis in organic solvents. Previously, we have demonstrated electrostatically grafted, telechelic PEGs encasing DNA are displaceable in the presence of a considerably high concentration of metal-cations.[36] Although the effect of various cationic species on the PEGylated structures is a matter of further investigation, we have adopted metal ions-induced dePEGylation to achieve the deactivation of the "supraG4zymes". The presence of 10 mM potassium phosphate buffer, 1.6 mM KCl, and 0.8 mM $MgCl_2$ resulted in the detachment of the PEG shell from CatG4-PEG350 and thus deactivated the biocatalyst in methanol (Figure S43).

DISCUSSION

The research unfolds the use of electrostatic PEGylation[36] to solubilize DNA in organic solvents. Such organic soluble PEGylated G-rich DNA molecules allowed the unprecedented formation of metal-free self-assembled supramolecular DNA G4s. This novel self-assembly behavior could primarily be attributed to the lower dielectric constant of the employed alcohols and the intrinsic crowding associated with the PEGylated strands.[39,63] Our ascription to the solvent dielectric relies on the study that puts forth details about primary aliphatic alcohols used as cosolvents that-induced stabilization of quadruplex structures in contrast to the destabilization of DNA duplexes in mixtures of these alcohols with water.[39] The medium selective structure formation observed (vide supra) reveals the necessity of lower dielectric constant for the folding of a PEGylated G-rich DNA in a solution devoid of metal ions. Additional factors involving the interaction between the hydrocarbons and ether groups of the PEG shell with the G-quartet via CH-π and lone-pair-π interactions might have contributed to the formation of the PEGylated structures by providing an enthalpic stabilization, as was previously observed in case of G4s obtained from tetraethylene glycol-modified deoxythymidines.[64,65] Substantial stacking interactions between G-quartets are expected due to the presence of several PEG chains on a single molecule of G-rich DNA.[65] The neutralization of the negative charges residing on the backbone of DNA by the charge-specific grafting of amino-terminated PEG polymers and close proximity of the ion pairs might have lowered the phosphate-phosphate repulsion energy and hence could have favored the enthalpic stabilization.[66] Moreover, decreased entropy of the system seems to have been facilitated by guanine association owing to the anticipated minimization in the electrostatic repulsion and increased stacking interactions.[66] The elucidation of the driving force enabling the formation of metal-free supramolecular DNA G4s using PEG-decorated G-rich sequences in organic solvents necessitates extensive investigations that are beyond the scope of the present study and shall be dealt with separately.

The described approach offers an effective platform to broaden the conformational landscape of the DNA G4s by enabling their easy modulation with considerable control over structural variability. An increase in the percentage of hybrid and/or antiparallel conformation is feasible by high-density grafting of PEG chains onto the phosphates of G-rich DNA whereas a systematic increase in the percentage of parallel conformation is achievable by increasing the molecular weight of the PEG shell. Strikingly, the designed supramolecular G-rich scaffolds together with hemin generate catalytically active species termed "supraG4zymes". The developed "supraG4zymes" allow materializing solvent-selective and structure-specific oxidative catalysis of ABTS in organic solvents. Although the use of electrostatic engineering to realize DNA-based chemistry in organic phase[26,27] and covalent PEGylation to achieve DNA-catalyzed oxidation in methanol[33] are known, we herein report the very first noncovalently engineered DNA biocatalyst that allows dictated catalytic transformations in organic solvents. Our findings may greatly accelerate the fabrication of engineered DNA G4s with desired properties and persuasively amplify the applicability of DNA-based supramolecular catalysts for various reactions in organic media.

Limitations of the study

The present contribution does not explore the feasibility of the charge-specific PEGylation strategy to solubilize longer DNA strands or investigate their sequence-specific folding. Moreover, the study lacks exploration into the DNA-catalyzed oxidation of organic substrates like dibenzothiophene (DBT), leaving an unaddressed area for further research in this domain.

STAR★METHODS

Detailed methods are provided in the online version of this paper and include the following:

- KEY RESOURCES TABLE
- RESOURCE AVAILABILITY
  - Lead contact
  - Materials availability
  - Data and code availability
- METHOD DETAILS
  - Synthesis and characterization of DNA and ANI.HCl
  - DNA-PEG complexation and characterization
  - Ultraviolet (UV) absorption spectroscopy
  - Sample preparation for CD measurements
  - CD spectroscopy
  - Normalization of CD spectra
  - NMR spectroscopy
  - SAXS measurements
  - Peroxidase activity measurements
  - Michaelis-Menten kinetics

SUPPLEMENTAL INFORMATION

Supplemental information can be found online at https://doi.org/10.1016/j.isci.2024.109689.

ACKNOWLEDGMENTS

We are grateful to Prof. B. L. Feringa and his group members for allowing us to use the JASCO J-810 spectropolarimeter. The authors are thankful to J. van der Velde for his contribution to the ICP-OES measurements. G.C. is indebted to the Erasmus Mundus Program for economic assistance through the NAMASTE scholarship. The research was financially supported by the European Union (European Research Council Advanced Grant SUPRABIOTICS No. 694610). Additional funding was provided by the National Institutes of Health GM077422 (to J.B.C).

AUTHOR CONTRIBUTIONS

Conceptualization, G.C. and A.H.; Methodology, G.C., K.B., and A.H.; Investigation, G.C., K.B., R.D.V.G., M.E., G.P., M.L., and W.J.N.K.; Writing – Original Draft, G.C., K.B., R.D.V.G., M.E., G.P., L.Z., T.W., J.B.C., and A.H.; Writing – Review and Editing, G.C., K.B., R.D.V.G., and A.H.; Funding Acquisition, J.B.C. and A.H.; Resources, M.L., R.D.V.G., J.B.C., and A.H.; Supervision, T.W., J.B.C., and A.H.

DECLARATION OF INTERESTS

The authors declare no competing interests.

Received: January 7, 2021
Revised: October 4, 2023
Accepted: April 5, 2024
Published: April 9, 2024

REFERENCES

1. Davis, J.T. (2004). G-quartets 40 years later: from 5′-GMP to molecular biology and supramolecular chemistry. Angew. Chem. Int. Ed. *43*, 668–698.
2. Sen, D., and Gilbert, W. (1988). Formation of parallel four-stranded complexes by guanine-rich motifs in DNA and its implications for meiosis. Nature *334*, 364–366.
3. Burge, S., Parkinson, G.N., Hazel, P., Todd, A.K., and Neidle, S. (2006). Quadruplex DNA: sequence, topology and structure. Nucleic Acids Res. *34*, 5402–5415.
4. Murat, P., and Balasubramanian, S. (2014). Existence and consequences of G-quadruplex structures in DNA. Curr. Opin. Genet. Dev. *25*, 22–29.
5. Ge, B., Huang, Y.C., Sen, D., and Yu, H.Z. (2010). A robust electronic switch made of immobilized duplex/quadruplex DNA. Angew. Chem. Int. Ed. *49*, 9965–9967.
6. Huang, Y.C., and Sen, D. (2014). A twisting electronic nanoswitch made of DNA. Angew. Chem. Int. Ed. *53*, 14055–14059.
7. Wang, F., Liu, X., and Willner, I. (2015). DNA switches: from principles to applications. Angew. Chem. Int. Ed. *54*, 1098–1129.
8. Kuzuya, A., and Tanaka, S. (2017). Hydrogels utilizing G-quadruplexes. MOJ Poly Sci. *1*, 201–203.
9. Travascio, P., Li, Y., and Sen, D. (1998). DNA-enhanced peroxidase activity of a DNA aptamer-hemin complex. Chem. Biol. *5*, 505–517.
10. Kosman, J., and Juskowiak, B. (2011). Peroxidase-mimicking DNAzymes for biosensing applications: a review. Anal. Chim. Acta *707*, 7–17.
11. Neo, J.L., Kamaladasan, K., and Uttamchandani, M. (2012). G-quadruplex based probes for visual detection and sensing. Curr. Pharm. Des. *18*, 2048–2057.
12. Tokura, Y., Harvey, S., Chen, C., Wu, Y., Ng, D.Y.W., and Weil, T. (2018). Fabrication of defined polydopamine nanostructures by DNA origami-templated polymerization. Angew. Chem. Int. Ed. *57*, 1587–1591.
13. Shamsi, M.H., and Kraatz, H.B. (2013). Interactions of metal ions with DNA and some applications. J. Inorg. Organomet. Polym. *23*, 4–23.
14. Bhattacharyya, D., Mirihana Arachchilage, G., and Basu, S. (2016). Metal cations in G-quadruplex folding and stability. Front. Chem. *4*, 38.
15. Campbell, N.H., and Neidle, S. (2012). G-quadruplexes and metal ions. Met. Ions Life Sci. *10*, 119–134.
16. Largy, E., Mergny, J.L., and Gabelica, V. (2016). Role of alkali metal ions in G-Quadruplex nucleic acid structure and stability. Met. Ions Life Sci. *16*, 203–258.
17. Gu, J., Leszczynski, J., and Bansal, M. (1999). A new insight into the structure and stability of Hoogsteen hydrogen-bonded G-tetrad: an ab initio SCF study. Chem. Phys. Lett. *311*, 209–214.
18. Ijiro, K., and Okahata, Y. (1992). A DNA-lipid complex soluble in organic solvents. J. Chem. Soc., Chem. Commun. 1339–1341.
19. Tanaka, K., and Okahata, Y. (1996). A DNA-lipid complex in organic media and formation of an aligned cast film. J. Am. Chem. Soc. *118*, 10679–10683.
20. Okahata, Y., Kobayashi, T., Tanaka, K., and Shimomura, M. (1998). Anisotropic electric conductivity in an aligned DNA cast film. J. Am. Chem. Soc. *120*, 6165–6166.
21. Fukushima, T., Hayakawa, T., Inoue, Y., Miyazaki, K., and Okahata, Y. (2004). Intercalation behavior and tensile strength of DNA-lipid films for the dental application. Biomaterials *25*, 5491–5497.
22. Liu, K., Chen, D., Marcozzi, A., Zheng, L., Su, J., Pesce, D., Zajaczkowski, W., Kolbe, A., Pisula, W., Müllen, K., et al. (2014). Thermotropic liquid crystals from biomacromolecules. Proc. Natl. Acad. Sci. USA *111*, 18596–18600.
23. Liu, K., Shuai, M., Chen, D., Tuchband, M., Gerasimov, J.Y., Su, J., Liu, Q., Zajaczkowski, W., Pisula, W., Müllen, K., et al. (2015). Solvent-free liquid crystals and liquids from DNA. Chem. Eur J. *21*, 4898–4903.
24. Liu, K., Varghese, J., Gerasimov, J.Y., Polyakov, A.O., Shuai, M., Su, J., Chen, D., Zajaczkowski, W., Marcozzi, A., Pisula, W., et al. (2016). Controlling the volatility of the written optical state in electrochromic DNA liquid crystals. Nat. Commun. *7*, 11476.
25. Liu, K., Zheng, L., Ma, C., Göstl, R., and Herrmann, A. (2017). DNA-surfactant complexes: self-assembly properties and applications. Chem. Soc. Rev. *46*, 5147–5172.
26. Rozenman, M.M., and Liu, D.R. (2006). DNA-templated synthesis in organic solvents. Chembiochem *7*, 253–256.
27. Liu, K., Zheng, L., Liu, Q., de Vries, J.W., Gerasimov, J.Y., and Herrmann, A. (2014). Nucleic acid chemistry in the organic phase: from functionalized oligonucleotides to DNA side chain polymers. J. Am. Chem. Soc. *136*, 14255–14262.
28. Abe, H., Abe, N., and Ito, Y. (2006). Structure analysis of oligonucleotide in organic solvent. Nucleic Acids Symp. Ser. *50*, 25–26.
29. Mok, H., and Park, T.G. (2006). PEG-assisted DNA solubilization in organic solvents for preparing cytosol specifically degradable PEG/DNA nanogels. Bioconjug. Chem. *17*, 1369–1372.
30. Ganguli, M., Jayachandran, K.N., and Maiti, S. (2004). Nanoparticles from cationic copolymer and DNA that are soluble and stable in common organic solvents. J. Am. Chem. Soc. *126*, 26–27.
31. Chen, W., Gerasimov, J.Y., Zhao, P., Liu, K., and Herrmann, A. (2015). High-density noncovalent functionalization of DNA by electrostatic interactions. J. Am. Chem. Soc. *137*, 12884–12889.
32. Tan, X., Lu, H., Sun, Y., Chen, X., Wang, D., Jia, F., and Zhang, K. (2019). Expanding the materials space of DNA via organic-phase ring-opening metathesis polymerization. Chem *5*, 1584–1596.
33. Abe, H., Abe, N., Shibata, A., Ito, K., Tanaka, Y., Ito, M., Saneyoshi, H., Shuto, S., and Ito, Y. (2012). Structure formation and catalytic activity of DNA dissolved in organic solvents. Angew. Chem. Int. Ed. *51*, 6475–6479.

34. Shibata, T., Dohno, C., and Nakatani, K. (2013). G-quadruplex formation of entirely hydrophobic DNA in organic solvents. Chem. Commun. *49*, 5501–5503.
35. Wang, Z., Zhao, J., Bao, J., and Dai, Z. (2016). Construction of metal-ion-free G-quadruplex-hemin DNAzyme and its application in S1 nuclease detection. ACS Appl. Mater. Interfaces *8*, 827–833.
36. Chakraborty, G., Balinin, K., Portale, G., Loznik, M., Polushkin, E., Weil, T., and Herrmann, A. (2019). Electrostatically PEGylated DNA enables salt-free hybridization in water. Chem. Sci. *10*, 10097–10105.
37. Kong, D.M., Cai, L.L., Guo, J.H., Wu, J., and Shen, H.X. (2009). Characterization of the G-quadruplex structure of a catalytic DNA with peroxidase activity. Biopolymers *91*, 331–339.
38. Cheng, X., Liu, X., Bing, T., Cao, Z., and Shangguan, D. (2009). General peroxidase activity of G-quadruplex-hemin complexes and its application in ligand screening. Biochemistry *48*, 7817–7823.
39. Smirnov, I.V., and Shafer, R.H. (2007). Electrostatics dominate quadruplex stability. Biopolymers *85*, 91–101.
40. Bugaut, A., and Balasubramanian, S. (2008). A sequence-independent study of the influence of short loop lengths on the stability and topology of intramolecular DNA G-quadruplexes. Biochemistry *47*, 689–697.
41. Lane, A.N., Chaires, J.B., Gray, R.D., and Trent, J.O. (2008). Stability and kinetics of G-quadruplex structures. Nucleic Acids Res. *36*, 5482–5515.
42. Kypr, J., Kejnovská, I., Renciuk, D., and Vorlícková, M. (2009). Circular dichroism and conformational polymorphism of DNA. Nucleic Acids Res. *37*, 1713–1725.
43. Balagurumoorthy, P., and Brahmachari, S.K. (1994). Structure and stability of human telomeric sequence. J. Biol. Chem. *269*, 21858–21869.
44. del Villar-Guerra, R., Trent, J.O., and Chaires, J.B. (2018). G-quadruplex secondary structure obtained from circular dichroism spectroscopy. Angew. Chem. Int. Ed. *57*, 7171–7175.
45. Joshi, D.R., and Adhikari, N. (2019). An overview on common organic solvents and their toxicity. J. Pharm. Res. Int. *28*, 1–18.
46. Wang, Y., and Patel, D.J. (1993). Solution structure of the human telomeric repeat d[$AG_3(T_2AG_3)_3$] G-tetraplex. Structure *1*, 263–282.
47. Mathad, R.I., and Yang, D. (2011). G-quadruplex structures and G-quadruplex-interactive compounds. Methods Mol. Biol. *735*, 77–96.
48. Chen, Y., and Yang, D. (2012). Sequence, stability, and structure of G-quadruplexes and their interactions with drugs. Curr. Protoc. Nucleic Acid Chem. *50*, Unit17.5.
49. Kikhney, A.G., and Svergun, D.I. (2015). A practical guide to small angle X-ray scattering (SAXS) of flexible and intrinsically disordered proteins. FEBS Lett. *589*, 2570–2577.
50. Vandavasi, V.G., Putnam, D.K., Zhang, Q., Petridis, L., Heller, W.T., Nixon, B.T., Haigler, C.H., Kalluri, U., Coates, L., Langan, P., et al. (2016). A structural study of CESA1 catalytic domain of Arabidopsis cellulose synthesis complex: evidence for CESA trimers. Plant Physiol. *170*, 123–135.
51. Ariyo, E.O., Booy, E.P., Patel, T.R., Dzananovic, E., McRae, E.K., Meier, M., McEleney, K., Stetefeld, J., and McKenna, S.A. (2015). Biophysical characterization of G-quadruplex recognition in the PITX1 mRNA by the specificity domain of the helicase RHAU. PLoS One *10*, e0144510.
52. Breßler, I., Kohlbrecher, J., and Thünemann, A.F. (2015). *SASfit*: a tool for small-angle scattering data analysis using a library of analytical expressions. J. Appl. Cryst. *48*, 1587–1598.
53. Svergun, D.I. (1992). Determination of the regularization parameter in indirect-transform methods using perceptual criteria. J. Appl. Cryst. *25*, 495–503.
54. Pollack, L. (2011). SAXS studies of ion-nucleic acid interactions. Annu. Rev. Biophys. *40*, 225–242.
55. Dvorkin, S.A., Karsisiotis, A.I., and Webba da Silva, M. (2018). Encoding canonical DNA quadruplex structure. Sci. Adv. *4*, 3007.
56. Canale, T.D., and Sen, D. (2017). Hemin-utilizing G-quadruplex DNAzymes are strongly active in organic co-solvents. Biochim. Biophys. Acta. Gen. *1861*, 1455–1462.
57. Bren, K.L. (2017). Engineered biomolecular catalysts. J. Am. Chem. Soc. *139*, 14331–14334.
58. Ruttkay-Nedecky, B., Kudr, J., Nejdl, L., Maskova, D., Kizek, R., and Adam, V. (2013). G-quadruplexes as sensing probes. Molecules *18*, 14760–14779.
59. Liu, J., Cao, Z., and Lu, Y. (2009). Functional nucleic acid sensors. Chem. Rev. *109*, 1948–1998.
60. Cano, A., Acosta, M., and Arnao, M.B. (2000). A method to measure antioxidant activity in organic media: application to lipophilic vitamins. Redox Rep. *5*, 365–370.
61. Dawidowicz, A.L., and Olszowy, M. (2013). The importance of solvent type in estimating antioxidant properties of phenolic compounds by ABTS assay. Eur. Food Res. Technol. *236*, 1099–1105.
62. Bhagavan, N.V., and Ha, C.E. (2015). Enzymes and enzyme regulation. In Essentials of Medical Biochemistry, pp. 63–84.
63. Nakano, S.i., Miyoshi, D., and Sugimoto, N. (2014). Effects of molecular crowding on the structures, interactions, and functions of nucleic acids. Chem. Rev. *114*, 2733–2758.
64. Tateishi-Karimata, H., Muraoka, T., Kinbara, K., and Sugimoto, N. (2016). G-quadruplexes with tetra(ethylene-glycol)-modified deoxythymidines are resistant to nucleases and inhibit HIV-1 reverse transciptase. Chembiochem *17*, 1399–1402.
65. Tateishi-Karimata, H., Ohyama, T., Muraoka, T., Podbevsek, P., Wawro, A.M., Tanaka, S., Nakano, S.I., Kinbara, K., Plavec, J., and Sugimoto, N. (2017). Newly characterized interaction stabilizes DNA structure: oligoethylene glycols stabilize G-quadruplexes CH-π interactions. Nucleic Acids Res. *45*, 7021–7030.
66. Kogut, M., Kleist, C., and Czub, J. (2016). Molecular dynamics simulations reveal the balance of forces governing the formation of a guanine tetrad-a common structural unit of G-quadruplex DNA. Nucleic Acids Res. *44*, 3020–3030.
67. del Villar-Guerra, R., Gray, R.D., and Chaires, J.B. (2017). Characterization of quadruplex DNA structure by circular dichroism. Curr. Protoc. Nucleic Acid Chem. *68*, 17.8.16.
68. Orthaber, D., Bergmann, A., and Glatter, O. (2000). SAXS experiments on absolute scale with Kratky systems using water as a secondary standard. J. Appl. Cryst. *33*, 218–225.
69. Humer, D., and Spadiut, O. (2019). Improving the performance of horseradish peroxidase by site-directed mutagenesis. Int. J. Mol. Sci. *20*, 916.

STAR★METHODS

KEY RESOURCES TABLE

REAGENT or RESOURCE	SOURCE	IDENTIFIER
Chemicals, peptides, and recombinant proteins		
4-(hexyloxy)anilinium chloride (ANI.HCl)	Synthesized, see method details	N/A
mPEG-Amine 350 Da	Creative PEGWorks	Catalog No.: PLS-2629
mPEG-Amine 750 Da	Sigma-Aldrich	CAS No.:80506-64-5
mPEG-Amine 2000 Da	Iris Biotech GmbH	Product Code: PEG1152
Methanol absolute AR grade (99.8 %)	Biosolve Chimie	CAS No.: 67-56-1
Ethanol absolute EMSURE® grade (99.9 %)*	Merck	CAS No.: 64-17-5
Ethanol puriss. grade (96.0-97.2 %)**	Sigma-Aldrich	CAS No.: 64-17-5
Dimethyl sulfoxide (DMSO) cell culture grade (99.5 %)	PanReac AppliChem	CAS No.: 67-68-5
Hemin from Porcine	Sigma-Aldrich	CAS No.: 16009-13-5
2,2′-Azino-bis(3-ethylbenzothiazoline-6-sulfonic acid) diammonium salt (ABTS)	Roche Diagnostics GmbH	CAS No.: 30931-67-0
10-acetyl-3,7-dihydroxyphenoxazine (Amplex Red)	Sigma-Aldrich	CAS No.: 119171-73-2
Hydrogen peroxide 30 % EMSURE® grade	Merck	CAS No.: 7722-84-1
Oligonucleotides		
ss22, 5′-CCTCGCTCTGCTAATCCTGTTA-3′	Synthesized, see method details	N/A
CatG4, 5′- TGGGTAGGGCGGGTTGGGAAA-3′	Biomers	N/A
CatG4RR, 5′-GGAGTGTGAGCGTGGAGAGTG-3′	Biomers	N/A
PS2.M, 5′-GTGGGTAGGGCGGGTTGG-3′	Synthesized, see method details	N/A
HT21, 5′-GGGTTAGGGTTAGGGTTAGGG-3′	Synthesized, see method details	N/A
Other		
Instrumentation	Commercial, see method details	N/A

*Used to prepare samples for absorbance, CD, and SAXS measurements.
**Used for the peroxidase activity measurements.

RESOURCE AVAILABILITY

Lead contact

Further information and requests should be directed to and will be fulfilled by the lead contact, Andreas Herrmann (herrmann@dwi.rwth-aachen.de).

Materials availability

This study did not generate new unique materials or reagents.

Data and code availability

- All data related to this paper will be shared by the lead contact upon reasonable request.
- This paper does not report original code.
- Any additional information required to reanalyze the data reported in this paper is available from the lead contact upon reasonable request.

METHOD DETAILS

Synthesis and characterization of DNA and ANI.HCl

The synthesis and purification of the DNA sequences designated as ss22, PS2.M, and HT21 were performed as described earlier.[36] These were synthesized using an ÄKTA OligoPilot 100 automated DNA synthesizer (GE Healthcare) at a 45 μmol scale on a universal solid support (Primer Support 5G UnyLinker 350, GE Healthcare) according to standard protocols. Deprotection and cleavage from the solid support were carried out in a 25 % ammonia solution (Boom B. V., Netherlands) at 65°C for 16 h. Purification of the oligos was performed on an ÄKTA Explorer (GE Healthcare) using a HiTrap Q HP 5 mL anion-exchange column (GE Healthcare) under a gradient of buffer A (10 mM NaOH; pH 12.0) and

buffer B (10 mM NaOH, 1 M NaCl; pH 12.0). The oligos were desalted after purification on a HiTrap Desalting 5 mL column (GE Healthcare) under an isocratic flow of 20 % ethanol. Finally, the oligos were filtered using a Whatman 0.45 μm syringe filter containing a cellulose acetate membrane. CatG4 and CatG4RR obtained from the commercial supplier (vide supra) were used without further purification. The identity and purity of the aforementioned oligos were confirmed by matrix-assisted laser desorption/ionization time-of-flight (MALDI-ToF) mass spectrometry (Figure S44). MALDI-ToF spectra were recorded on a Voyager-DE™ PRO Biospectrometry™ Workstation (Applied Biosystems). The synthesis of 4-(hexyloxy)anilinium chloride (ANI.HCl) was carried out as per the published procedure.[31,36] In brief, 4-(hexyloxy)aniline (25 g, 130 mmol) was placed in a 1000 mL round-bottom flask equipped with a magnetic stir bar. 500 mL of diethyl ether was added. 4-(hexyloxy)aniline was allowed to dissolve completely under vigorous stirring. Freshly prepared hydrochloride gas, obtained by mixing NaCl with H_2SO_4, was passed into the solution of 4-(hexyloxy)aniline. A turbid solution was observed after a few minutes of stirring, and a precipitate was formed. The solution was flushed with hydrochloride for another 30 minutes, and then the reaction was ceased. Subsequent to the collection of the precipitate by filtration, it was rinsed with diethyl ether (2 × 300 mL). The purple-colored solid was dried overnight under vacuum (27.4 g, ~ 92 % yield). ^{1}H NMR spectrum was obtained to confirm the identity and purity of ANI.HCl (Figure S45).

DNA-PEG complexation and characterization

DNA-ANI and subsequently DNA-PEG complexes were synthesized according to the published protocol.[36] In brief, ANI.HCl (three equivalents to the charge of DNA) dissolved in ultrapure water was added to the tube containing 1.5 μmol of the aqueous solution of the desired single-stranded DNA. The resulting solution was mixed thoroughly and consequently the insoluble DNA-ANI complex precipitated from the aqueous phase. The treated DNA-ANI complex was freeze-dried overnight and resuspended in methanol. A solution containing an excess amount of mPEG-Amine dissolved in methanol was added to the dispersed DNA-ANI solution. After the complete exchange of ANI molecules by cationic amino PEG chains, the complex solution was diluted by adding ultrapure water. This entire solution was transferred to a molecular weight cut-off tube and concentrated by centrifugation. The concentrated DNA-PEG complex solution was subjected to purification employing a 1:1 water-methanol mixture to remove the unreacted PEG and free ANI molecules. The final DNA-PEG complex was obtained after freeze-drying. The synthesized complex was characterized by ^{1}H NMR. The stock concentration of each PEG-modified oligonucleotide was calculated by following the previously described method that relies on the grafting stoichiometry of PEG chains onto the DNA backbone, determined from ^{1}H NMR spectroscopy.[36] To explain, the freeze-dried form of each DNA-PEG complex was individually weighed (up to six digits after the decimal). The molecular weights of the complexes were calculated as follows:

$$\text{Molecular weight of ss22-PEG350} = 6612 + 21 \times 350 = 13,962\ \text{g/mol}$$

$$\text{Molecular weight of CatG4-PEG350} = 6647 + 20 \times 350 = 13,647\ \text{g/mol}$$

$$\text{Molecular weight of CatG4-PEG750} = 6647 + 20 \times 750 = 21,647\ \text{g/mol}$$

$$\text{Molecular weight of CatG4-PEG2000} = 6647 + 20 \times 2000 = 46,647\ \text{g/mol}$$

$$\text{Molecular weight of CatG4RR-PEG350} = 6647 + 20 \times 350 = 13,647\ \text{g/mol}$$

$$\text{Molecular weight of PS2.M-PEG350} = 5707 + 17 \times 350 = 11,657\ \text{g/mol}$$

$$\text{Molecular weight of HT21-PEG350} = 6653 + 20 \times 350 = 13,653\ \text{g/mol}$$

It is well-known that C = n/V; here
C = concentration (moles/L= molarity)
n = moles of solute (DNA-PEG complex)
V = volume of solution in L

The amount of each DNA-PEG complex (in moles) was obtained by dividing the weighed mass (m) of the DNA-PEG complex with its molecular weight (M), n = m/M. All the DNA-PEG stocks were prepared to be of 3 mM by adding ultrapure water to the respective complexes. ICP-OES was performed on a Perkin Elmer Optima 7000 DV. The standards and samples were prepared as described earlier.[36] Yttrium (Y) standard 1000 mg/L (PerkinElmer, N9303810) was used for internal standard and ICP multi-element standard solution IV 1000 mg/L (No. 1.11355.0100, Merck KGaA, Germany) was used to prepare the three different standards (Standard 1: 1 ppm, Standard 2: 5 ppm, and Standard 3: 10 ppm) against which each sample was measured. The standards and samples were prepared in a 2 % nitric acid solution. The samples were diluted six-fold with the 2 % nitric acid solution. Double-distilled water was used for the preparation of the 2 % nitric acid solution. The calibration blank is the 0 mg/L standard, and the most sensitive wavelength was used for the analysis.

Ultraviolet (UV) absorption spectroscopy

The absorbance spectra were acquired on a V-630 UV-Vis spectrophotometer (JASCO Benelux B. V.) using a quartz cuvette with 1 cm light-path. 200 μM stocks were prepared in ultrapure water from the original 3 mM stock solution of ss22-PEG350 complex and were freeze-dried

overnight. The lyophilized powders were redissolved in methanol and ethanol, individually and were allowed to shake at 800 rpm for 1 h at room temperature to obtain 200 μM stocks in the employed organic solvents. The obtained stocks were diluted with the respective organic solvent to achieve the specified concentrations.

Sample preparation for CD measurements

100 μM of the DNA (CatG4 or CatG4RR) was mixed with 200 mM Tris-HCl (pH 7.5), 32 mM KCl, and 16 mM $MgCl_2$ whereas 50 μM of the oligonucleotide (PS2.M or HT21) was added to 250 mM Tris-HCl (pH 7.5), 1.5 M NaCl and 200 mM KCl. 100 μM of the PEGylated oligos were prepared in ultrapure water from their original 3 mM stock solutions. All the reaction mixtures were mixed thoroughly and heated to 90°C for 10 minutes and cooled to 25°C with a rate of 2°C/min using a Mastercycler (Eppendorf). Subsequently, the samples were incubated at 4°C for 2 hours. The samples were freeze-dried overnight and redissolved in ultrapure water (non-PEGylated DNA) or absolute methanol/ethanol (PEGylated oligos) to achieve the aforesaid respective DNA concentrations. The resulting reaction mixtures were allowed to shake at 800 rpm for 1 h at room temperature to ensure the formation of homogeneous solutions. The obtained solutions were diluted with the desired solvent to achieve the required concentrations.

CD spectroscopy

CD spectra were recorded on a JASCO J-810 spectropolarimeter using a 1 cm path-length quartz cuvette following a previously described protocol.[67] The parameters used to record the CD spectra were: 230-320 nm wavelength range, 1 nm data pitch, 1 nm bandwidth, 0.5 sec response, standard sensitivity, and 100 nm/min of scanning speed. Each spectrum is an average of 5 accumulations and the spectral contribution from the buffer or pure organic solvent was subtracted. The obtained spectra were smoothed to facilitate comparisons. Melting experiments were performed on a JASCO J-1500 CD spectrometer. The samples in the buffer, methanol, and ethanol were heated from 5°C to 95°C, 65°C, and 80°C, respectively. The temperature interval in each case was 5°C and the ramp rate was 1°C/min with other parameters the same as mentioned above. A reaction mixture composed of 5 μM of the DNA (CatG4 or CatG4RR), 10 mM Tris-HCl (pH 7.5), 1.6 mM KCl, and 0.8 mM $MgCl_2$ or a solution containing 5 μM of the oligonucleotide (PS2.M or HT21), 25 mM Tris-HCl (pH 7.5), 150 mM NaCl, and 20 mM KCl was used to record the CD spectra/melts of the unmodified oligos. 5 μM of the DNA in the preferred organic solvent was used to acquire the CD spectra/melts of the PEGylated sequences unless specified otherwise.

Normalization of CD spectra

All the CD spectra were normalized to $\Delta\varepsilon$ ($M^{-1}.cm^{-1}$) = θ/(32980 × c × l) based on strand concentration of the G-quadruplex, θ is the CD ellipticity in millidegrees, c is the concentration of DNA expressed in mol/L and l is the path-length in cm.

NMR spectroscopy

The ^1H NMR spectra of the solutions in D_2O for the investigation of the DNA PEGylation and the sample in DMSO-d_6 to ensure the identity as well as purity of ANI.HCl was recorded on a Varian Mercury NMR spectrometer operating at 400 MHz. The NMR spectra showing the imino regions with CD_3OH as a solvent were recorded at 600 MHz using a Bruker Avance NMR spectrometer. Here, for the temperature-dependent experiments, the -OH peak was suppressed using a 3-9-19 pulse sequence with gradients (WATERGATE), the delay for binomial suppression was set to 250 μs. The other spectra showing the imino region were recorded using a 1-3-3-1 pulse sequence (jump-and-return method) with a delay for binomial water suppression of 90 μs. The relaxation delay was set to 2.0 s and the acquisition time to 3.6 s.

SAXS measurements

SAXS studies were performed using the MINA X-ray instrument at the University of Groningen. X-rays of 8 keV (wavelength λ = 1.5413 Å) are generated by a rotating anode functioning at 45 kV and 60 mA. SAXS 2D patterns were acquired using a Vantec Bruker detector placed at two different sample-to-detectors distances (S-to-D = 24 and 300 cm, respectively). The peak positions from a standard silver behenate sample were used to calibrate the angular range 2θ. The final reaction mixture used for SAXS measurements was composed of 0.4 mm of the oligonucleotide in the designated organic solvent or 50 mM Tris-HCl (pH 7.5), 100 mM KCl and 5 mM $MgCl_2$. The samples were annealed, incubated, and redissolved by following the protocol used to prepare CD samples. 1.5 mm Mark-tubes made of borosilicate glass (Hilgenberg GmbH) were filled with 30 μL of the respective solution. The capillary end was flame-sealed to avoid solvent evaporation over time. Prior to the radial integration, 2D patterns were normalized by their exposure time, sample transmission, and background subtraction were performed. The scattering intensity from the capillary plus the buffer with the appropriate quantities of salts or pure methanol/ethanol was used as a background for the respective sample. The corrected patterns were analyzed using Fit2D and a Matlab code and the curves are finally reported as scattering intensity I(q) vs the modulus of the scattering vector $q = (4\pi/\lambda)\sin\theta$. The two curves acquired at different S-to-D were finally merged using Matlab. Calibration to the absolute scale in cm^{-1} was achieved by the secondary standard method, using water as intensity standard.[68]

Peroxidase activity measurements

The non-PEGylated and PEG-grafted oligos were annealed in aqueous medium at the specified ionic strength or in ultrapure water, respectively by heating to 90°C for 10 minutes and cooled to 25°C with a rate of 2°C/min. The samples were incubated at 4°C for 2 hours.

Subsequently, the solutions were lyophilized overnight. Ultrapure water or methanol/ethanol was added to the respective reaction mixtures and the resulting solutions were allowed to shake at 800 rpm for 1 h at room temperature. Hemin (dissolved in DMSO) was then added and the solutions were kept at room temperature for 30 minutes with mild shaking. ABTS (dissolved in methanol) or Amplex Red (dissolved in DMSO) was added and mixed thoroughly. The oxidation was initiated by the addition of H_2O_2. All the experiments dealing with the activity measurements were performed in microtiter plates using SpectraMax M3 (Molecular Devices) at room temperature. All the absorbance spectra were recorded at 15 minutes from the addition of H_2O_2, whereas the kinetics were followed by monitoring the appearance of the ABTS radical cation ($ABTS^{\cdot+}$) at 414 nm or by measuring the absorbance changes at 570 nm associated with oxidation of Amplex Red[56] immediately after the addition of H_2O_2. Triplicate measurements were conducted in all the experiments dealing with the time-dependent absorbance changes at 414 nm or at 570 nm. The absorbance contributed by the participating DNA-hemin complex with proper quantities of salts or pure methanol/ethanol was respectively subtracted in all the spectra measurements. Background subtraction in kinetics measurements was done only in the case of experiments dealing with varying DNA concentrations. The final composition of the mixture was 5 μM DNA, 10 mM potassium phosphate (pH 7.0), 1.6 mM KCl, 0.8 mM $MgCl_2$, 5 μM hemin, 1 mM ABTS and 1 mM H_2O_2 or 5 μM DNA-PEG complex, 5 μM hemin, 1 mM ABTS or 1 mM Amplex Red and 1 mM H_2O_2 for aqueous and organic media respectively unless mentioned otherwise.

Michaelis-Menten kinetics

Time-dependent absorbance changes at 414 nm reflecting oxidation of 0.2 mM, 0.4 mM, 0.6 mM, 0.8 mM, 1.0 mM, 1.2 mM, 1.4 mM, 1.6 mM, 1.8 mM, and 2.0 mM of ABTS catalyzed by CatG4-PEG350-hemin complex in methanol were recorded in triplicates following the method described above. The obtained absorbances were converted to corresponding concentrations of ABTS by using the Beer-Lambert law ($[ABTS] = A_{414\ nm} / (36000\ M^{-1}\ cm^{-1} * 0.87\ cm)$). The employed values of molar extinction coefficient[9] and path length[69] were adopted from the cited articles. The kinetic parameters (V_{max} and K_m) were obtained by fitting the initial rate (V_0) vs [ABTS] to the Michaelis-Menten equation (Equation 1) using nonlinear least squares fitting in Origin 2015 Data Analysis and Graphing Software. The initial rates were determined by a linear fitting of the initial linear portion (0 - 240 s) of the increase in absorbance.

$$V_0 = V_{max}[ABTS] / (K_m + [ABTS]) \quad \text{(Equation 1)}$$